# Highly Efficient Sequestration of (Radio) Iodine from Water via Isostructural ionic Metal-Organic Frameworks

A Thesis

Submitted in Partial Fulfilment of the Requirements for the Degree of

**Bachelor of Science and Master of Science (BS-MS)**

By

Rafael Tayung


Indian Institute of Science Education and Research Pune

Dr. Homi Bhabha Road,

Pashan, Pune 411008, INDIA.

**March 2025**

**Supervisor: Prof. Sujit K Ghosh**

**Rafael Tayung**

**20201208**

# Certificate

This is to certify that this thesis entitled "***Highly Efficient Sequestration of (Radio) Iodine from Water via Isostructural ionic Metal-Organic Frameworks***" towards the partial fulfillment of the Master's degree program at the Indian Institute of Science Education and Research, Pune represents research work carried out by **Rafael Tayung** (20201208) at the Indian Institute of Science Education and Research under the supervision of **Prof. Sujit K. Ghosh,** Department of chemistry, during the academic year 2024-2025.

**Prof. Sujit K. Ghosh**

Research Supervisor

E-mail: sghosh@iiserpune.ac.in

Contact No: +91(20)25908076

**Dr. Debangsu Sil**

Thesis Advisory Committee

E-mail: debangsu@iiserpune.ac.in

Contact No: +91-20-25908562

My thesis is dedicated to my beloved parents, **Maa** and **Papa**

# Declaration

I hereby declare that the matter embodied in the report entitled '***Highly Efficient Sequestration of (Radio) Iodine from Water via Isostructural Ionic Metal-Organic Frameworks***' are the results of the work carried out by me at the Department of Chemistry, Indian Institute of Science Education and Research, Pune, under the supervision of Prof. Sujit K Ghosh and the same has not been submitted elsewhere for any other degree. Wherever others contribute, every effort is made to indicate this clearly, with due reference to the literature and acknowledgment of collaborative research and discussions.

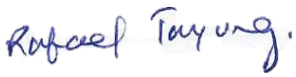

Rafael Tayung
Reg. No: 20201208
Date: 25-03-2025

# Table of Contents

# List of Figure

# List of Tables

# Acknowledgment

I would like to thank my supervisor, **Prof. Sujit K. Ghosh**, with my warmest gratitude for giving me the wonderful chance to work on my master's thesis under his supervision. It has been a great privilege to work under his supervision, and his valuable guidance and discussions enabled me to complete my thesis project and will assist me in the future, too. Working under his research group clarified my comprehension and provided me with self-confidence and inspiration that would last for a lifetime.

I am highly grateful to the current Director of IISER, Prof. Sunil S. Bhagwat, and the chair of the Chemistry Department, Prof. Nirmalya Ballav, for all the research facilities and lively academic environment. I am grateful to my thesis advisory committee member, Dr. Debangsu Sil, for his helpful suggestions and inputs, which contributed significantly to making my research a success. My heartfelt gratitude to the IISER Pune faculty members for their outstanding teaching and for inculcating a good research culture in me.

My research experience has been greatly enriched by the members of the SKG lab. I am especially thankful to my thesis advisor, Mr. Kishalay Biswas, for his ever-readiness, thoughtful suggestions, and guidance. I also want to acknowledge the contribution of members of the SKG lab, Dr. Gourab K. Dam, Dr. Sagarmani Rasaly, Dipanjan Majumdar, Anirban Roy, Dipayan Ghosh, Nayan Sarkar, Sudip Maity, Supriti Mahanta, Avijit Malakar, Sukalyan Chatterjee, and my friends Shalu Rana and Riddhi Saikia, for their suggestions and useful inputs at various stages of my research journey. Their coordination and support greatly contributed to shaping my work. In the end, I would like to express my gratitude towards my Maa and Papa for their support and belief in me.

# Abstract

Large-scale production of radioactive iodine isotopes ($^{129}I$ and $^{131}I$) in nuclear reactors is a serious environmental and health hazard in fallout situations, which requires the synthesis of highly effective iodine sequestration materials. This study utilized two isostructural ionic metal-organic frameworks (MOFs) iMOF-3C and IPM-201 with different counter anions for the selective removal of $I_2/I_3^-$ species. Both MOFs had fast kinetics, with capture efficiencies of over 99% within the initial 5 minutes of exposure. These results illustrate an adequate and stable method of the fast sequestration of radioactive iodine, with implications for their use in nuclear waste treatment. Both the MOFs are stable and porous for a wide range of pH as well as varied conditions of water. They therefore are highly efficient in charge- and size-selective entrapment of iodine via an ion-exchange process. The highest capacities of iMOF-3C and IPM-201 for iodine uptake in the vapor phase are 4.44 g $g^{-1}$ and 4.21 g $g^{-1}$, while in the aqueous phase, they are 3.28 g $g^{-1}$ and 2.54 g $g^{-1}$, respectively.

# 1. Introduction

## 1.1 Porous Materials

Porous materials are substances that contain space or void within their structure. This material is also found in various forms, such as rocks, soil, and biological tissues. Naturally occurring porous materials include pumice, zeolite, sandstone, charcoal, and coral reefs. This porous material is mainly used for water purification, filtration, and cooling systems, dating back to ancient Egyptian times.[1] However, naturally occurring porous materials have several drawbacks despite their usefulness. These drawbacks include mechanical strength, chemical stability, tunability, functionality, etc. These drawbacks make them less suitable for specific applications where more precise and reliable materials are required. So, another class of porous material is **Advanced Porous Material (AMP).** These materials are classified into three categories depending on the pore size. Material having less than 2 nanometers (nm) are referred to as microporous materials, while those within the pore size range between 2 nanometers to 50 nanometers are referred to as mesoporous, and the pore size larger than 50 nanometers are called microporous. These APMs consist of a broad spectrum of materials such as metal-organic frameworks (MOFs), metal-organic gel (MOG), metal-organic polyhedra (MOPs), porous organic materials (POMs), etc. This broad spectrum.

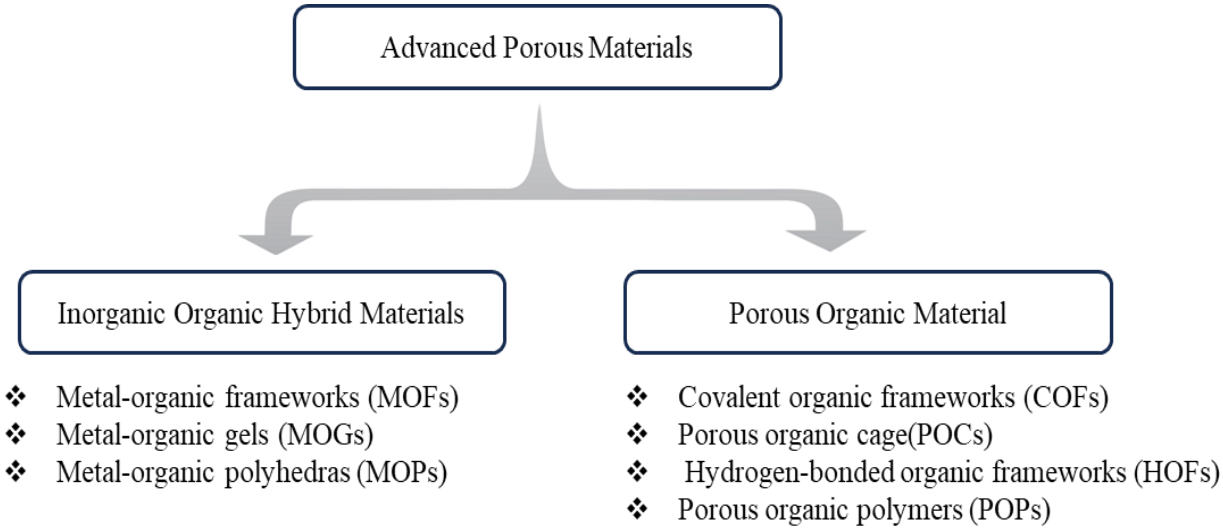


Figure 1.1 Schematic representation for classification of various types of advanced functional materials

of materials is subdivided into two categories: Inorganic-Organic hybrid Porous Materials and Porous Organic Materials (fig 1.1). Inorganic -Organic hybrid Porous Materials are crystalline made up of metal and organic building blocks. Other hand Porous organic materials are made up of organic building blocks that are strongly connected by strong covalent bonds and they are amorphous.

These APMs are engineered at the nano or micro-scale to exhibit specific and desirable properties. APMs are constructed by connecting inorganic /organic nodes and organic linkers via coordination or covalent bonds. By sophisticated selection of the building blocks and the underlying network topology, the shapes and sizes of the nanopores are carefully tailored selectively for particular applications. Control synthesis of these materials makes them promising materials in applications such as gas separation and storage, energy conversion, pollutant removal, biomedicine, and catalysis.[2]

### 1.2 Metal-organic frameworks (MOFs)

Metal-organic frameworks are a subclass of advanced porous materials (APMs) that have drawn special recognition for their distinct advantage over traditional porous materials, which include mesoporous silica, activated carbon, and zeolites. MOFs are porous crystalline solids constructed due to coordination bonds connecting inorganic metal nodes/clusters and organic ligands. During the formation of MOFs, solvent molecules in the reaction medium generally occupy the void space created by the framework. To access that void in frameworks, it is necessary to remove guest molecules, and this can be done by de-solvation by vacuum treatment or heating. These MOFs can be synthesized using another technique called “post-synthetic modification” (PSM), in which MOFs are created using the pre-synthetic method described above and contain functional subunits used to undergo chemical modification to create porous MOFs that are identical but have different functions.

Depending on the nature of the frameworks, metal-organic frameworks can be classified into neutral MOFs and ionic MOFs (i-MOFs). The frameworks can be strategically modified depending on the organic linker used in MOF synthesis. Neutral MOFs are formed when anionic carboxylate ligands bind with cationic metal nodes, creating a balanced framework. On the other hand, ionic MOFs are branched into two types based on their electrostatic nature: cationic and anionic frameworks. Cationic

frameworks form when N-donor ligands and positively charged metal centers are used, and additional counter anions neutralize the positively charged framework. In contrast, anionic MOFs are formed when positively metal-charged nodes fail to balance the charge after coordinating with ligands containing multiple anionic sites. In this case, the anionic charge is balanced by additional countercations.

Because of their characteristic structure and large surface area, MOFs are found in various applications such as gas storage and separation from a mixture of gases, as they include separation of greenhouse gases like carbon dioxide, methane, etc. Due to the functional properties of frameworks, MOFs are also used in heterogeneous catalysis. Extra ions in the ionic framework help in exchange-based applications, and also access to pores in frameworks helps in absorption and adsorbent applications.

### 1.3 Radioactive iodide: Challenges and concerns

Nuclear power is increasingly recognized as a clean and efficient energy source, playing a crucial role in addressing the rising global energy demand while supporting the transition toward carbon neutrality. However, a major challenge associated with nuclear energy is the safe management of radioactive waste, particularly volatile radionuclides such as iodine isotopes ($^{129}$I and $^{131}$I).[3,4] These isotopes are primarily generated as fission products of plutonium-239 and uranium-235 in nuclear reactors and are released during nuclear fuel reprocessing.[5,6] They predominantly exist as elemental iodine, with smaller fractions forming organic and metal iodides, which significantly complicates their containment and disposal.[7] The environmental and health risks associated with these iodine isotopes are particularly severe due to their volatility and ability to disperse easily through the atmosphere. Among them, $^{129}$I poses a significant long-term threat due to its ultra-long half-life (~16 million years), high toxicity, and strong mobility in geological environments, making its containment a persistent challenge.[8,9] On the other hand, $^{131}$I, while having a much shorter half-life (~8 days), is highly radioactive and can interfere with human metabolic processes, particularly affecting the thyroid gland and increasing the risk of radiation-induced diseases.[10-12] In aqueous environments, $^{129}$I commonly exists as molecular iodine ($I_2$) and triiodide ($I_3^-$) through redox equilibrium ($I_2 + I^- \rightleftharpoons I_3^-$). These species, due to their volatility at ambient temperatures and high solubility, can rapidly enter the hydrosphere and biosphere, leading to widespread contamination.[13-15] The Chornobyl disaster

provided a striking example of how volatile radionuclides, including $^{129}I$ and $^{131}I$, were dispersed across Europe, with significant accumulation in water bodies and subsequent bioavailability to living organisms.[16] The mobility of these isotopes allows them to be incorporated into food chains, exacerbating the risk of human and ecological exposure. Additionally, iodine radionuclides are not only byproducts of nuclear power plants but are also released from medical and industrial sources. $^{131}I$, extensively used in oncological treatments, can enter wastewater systems, contributing to secondary contamination.[17] Recent advancements in iodine speciation studies have revealed the complex physicochemical interactions governing its behavior in both gaseous and aqueous phases. These findings underscore the necessity for advanced containment, sequestration, and remediation strategies to mitigate the risks associated with radioactive iodine. Effective nuclear waste management, coupled with an insightful understanding of iodine chemistry, is essential to minimize environmental dispersion and protect human health from long-term radiation exposure.

### 1.4 Advanced porous materials for iodine sequestration:

Conventional adsorbents such as porous activated carbon and zeolites have been widely employed due to their cost-effectiveness, ease of availability, and strong affinity for iodine. However, these materials often suffer from suboptimal performance, particularly in aqueous systems, where their iodine uptake capacity is relatively low. This limitation underscores the necessity of designing next-generation sorbents with superior adsorption properties. In recent years, substantial research efforts have been directed toward the development of advanced porous materials for the efficient sequestration of iodine from contaminated environments.[18-22] Substantial progress has been achieved in enhancing adsorption kinetics, capacity, high-temperature capture, and selectivity. Despite these advances, there remains a critical need for the design of novel materials with enhanced iodine uptake efficiency to overcome the limitations of existing adsorbents. Over the past decade, a diverse class of porous sorbents, comprising both amorphous and crystalline frameworks—including metal-organic frameworks (MOFs),[23-26] covalent-organic frameworks (COFs),[27-29] and porous organic polymers (POPs)[30-34] has been extensively studied for their efficacy in iodine capture, owing to their tunable porosity, high surface area, and tailored host-guest interactions. A fundamental aspect of optimizing iodine capture involves

elucidating the underlying adsorption mechanisms at the molecular level. Most reported iodine adsorbents are charge-neutral and primarily interact with iodine via weak charge-transfer interactions, which can limit their overall efficiency. Therefore, the development of advanced sorbents that integrate multiple synergistic interactions, such as a combination of electrostatic forces and host-guest interactions, could significantly enhance the adsorption performance. Moving forward, the rational design of porous materials with tailored functionalities, such as tunable pore environments, high surface areas, and electrostatic active sites, holds great promise for toxic iodine sequestration.

To address the critical challenge of iodine sequestration, our study focuses on the development and investigation of ionic metal-organic frameworks (iMOFs) as advanced host materials for the efficient capture of molecular iodine ($I_2$) from vapor phase and triiodide ($I_3^-$) from aqueous media. iMOFs offer a unique advantage over conventional porous materials due to their intrinsic charged frameworks, high physicochemical stability, and structurally tunable backbones, making them a promising platform for the rational design of next-generation iodine sorbents. In this work, we report the synthesis and systematic evaluation of two isostructural iMOFs, namely iMOF-3C and IPM-201, which differ in their incorporated counteranions. While iMOF-3C features sulfate ($SO_4^{2-}$) as the charge-balancing anion, IPM-201 incorporates biphenyl sulfonic acid (BPSA), introducing an organic component to the framework. By leveraging these structural variations, we aim to elucidate the fundamental role of counter anions, both inorganic and organic, in governing the adsorption efficiency, selectivity, and underlying interactions responsible for iodine sequestration. Furthermore, to validate the real-world applicability of these materials, we extend our investigation to diverse environmental conditions. This includes assessing their iodine removal efficiency across complex aqueous matrices, evaluating the impact of competing anions that commonly coexist in natural and industrial effluents, and exploring their stability and performance across a broad pH range. The insights gained from this study are expected to contribute to the strategic

design of next-generation iMOFs with enhanced capture capabilities for environmental remediation and nuclear waste management.

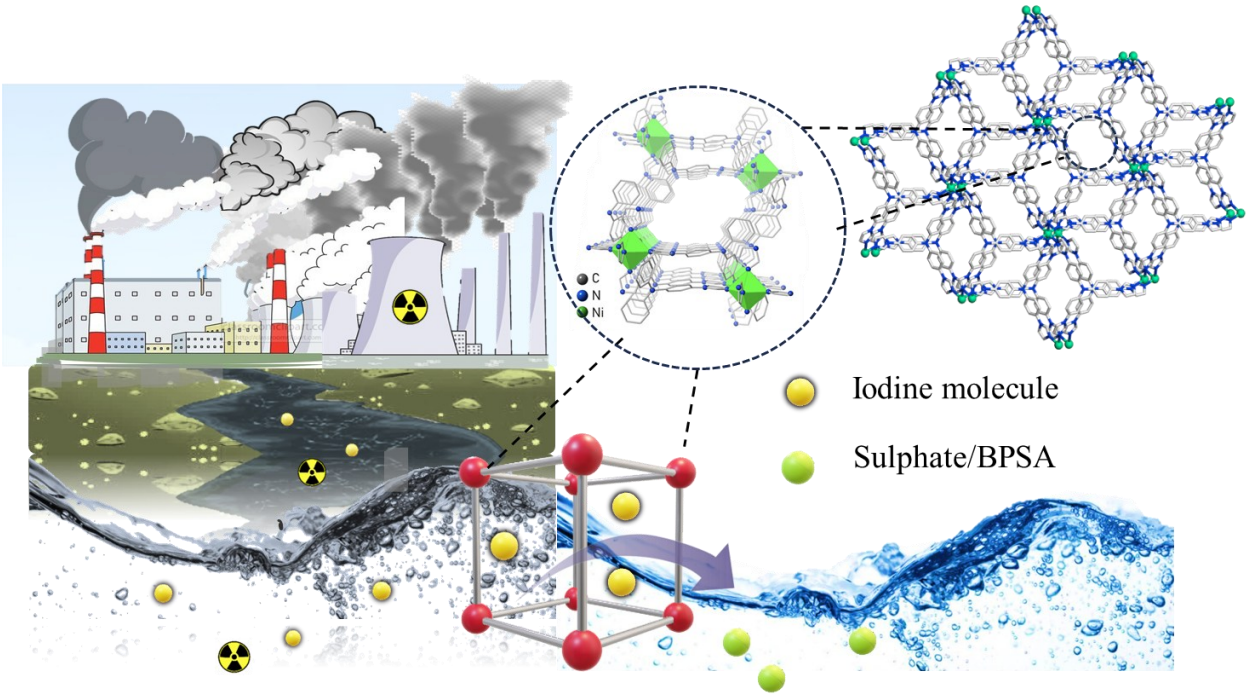


Figure 1.2: Schematic representation of selective capture of radioactive iodine by iMOFs

## 2. Materials and Methods

### 2.1 Materials

Depending on availability, all the reagents and solvents were commercially purchased from Sigma-Aldrich, TCI chemicals, Spectrochem, and Rankem and used without further purification.

### 2.2 General characterizations and physical measurements:

**2.2.1 Single crystal X-ray diffraction:** Single-crystal X-ray data of compound iMOF-3C was collected at 100 K on a Bruker D8 Venture Duo X-ray diffractometer equipped with Microfocus X-ray source (operated at 50 W; 50 kV/1 mA), graded multilayer optics for monochromatic Mo Kα radiation (λ = 0.71073 Å) focused X-ray beam and Photon 100 CMOS chip-based detector system

**2.2.2 Powder X-ray diffraction (PXRD):** Powder X-ray diffraction analyses were performed on a Burker D8 Advanced X-ray diffractometer at room using Cu Kα radiation (λ=1.5406 Å) in 5° to 40° 2θ with a scan speed of 1.2 $min^{-1}$.

**2.2.3 Thermogravimetric analysis (TGA):** Thermogravimetric analysis profiles were recorded on a Perkin Elmer STA 600 TGA analyzer by heating the sample from 30°C to 800°C under $N_2$ atmosphere with a heating rate of 10° $min^{-1}$.

**2.2.4 Fourier transform infrared spectroscopy (FT-IR):** The FT-IR were acquired by using NICOLET 6700 FT-IR spectrophotometer using KBr pellet in 500-4000 $cm^{-1}$ range.

**2.2.5 Field emission scanning electron microscopy (FE-SEM):** The morphology of the materials was investigated with a Zeiss Ultra Plus field-emission scanning electron microscope (FESEM) with an integral charge compensator and embedded EsB and AsB detectors (Oxford X-max instruments 80 mm2 (Carl Zeiss NTS, GmbH). The elemental analysis was carried out using a voltage of 15 KV equipped with an EDX detector. Data acquisition was performed with an accumulation time of >600s.S1.2.5 N2 and CO2 gas adsorption-desorption: measurements were performed using the BelSorp-Max instrument (Bel Japan). Prior to adsorption measurements, the activated samples were heated at 100 °C under vacuum for 08 hours using BelPrepvacII.

**2.2.6 X-ray photoelectron spectroscopy (XPS):** X-ray photoelectron spectroscopy was recorded using the K-Alpha+model (Thermo Fischer Scientific, UK) with Al Kα source.

**2.2.7 $CO_2$ adsorption-desorption isotherm measurements:** $CO_2$ gas adsorption-desorption measurements were performed using the BelSorp-Max instrument (Bel Japan). Before adsorption measurements, the activated samples were heated at 120°under a vacuum for 12 hours using BelPrepvac Ⅱ

**2.2.8 Diffuse reflectance spectroscopy:** DRS spectra and corresponding absorbance spectra were collected on a Shimadzu UV-3600i UV/Visible/NIR Spectrophotometer with the solid sample.

**2.2.9 Roman spectroscopy:** Raman spectra were measured with Xplora PLUS Raman microscope (Horiba Company) (633 nm laser and a 1200 lines/mm grating)

## 2.3 Experimental section

**General Consideration:** The aqueous triiodide ($I_3^-$) solution was prepared by dissolving a specific quantity of solid iodine and potassium iodide in deionized water. Various concentrations were achieved by diluting the stock solution with the appropriate amounts of distilled water unless stated otherwise. The concentrations of $I_3^-$ during all the experiments were detected by UV-vis spectroscopic analysis. All the adsorption experiments were performed at ambient conditions. All the data has been collected three/two times through UV-vis analysis to plot the final adsorption results.

**Vapor phase static iodine uptake studies:** A small glass vial containing 10 mg of MOFs was exposed to molecular iodine for 24 hours at 75 °C in a closed system. After the designated adsorption period, the vial was removed, allowed to cool to room temperature, and then weighed. The iodine uptake capacity of the compound was determined by calculating the weight difference of the vial before and after adsorption using the following formula:

$$W = \frac{(m_2 - m_1)}{m_1} \quad \text{..... (1)}$$

Where w (g.g-1) is the adsorption capacity of iodine uptake, $m_1$ (g) and $m_2$ (g) is the mass of compounds with the glass vial before and after being exposed to iodine vapor. The values of uptake capacity are the average values of at least three experiments.

**Sorption kinetic studies towards $I_3^-$:** For the time-dependent study for $I_3^-$ removal, we took 3 mL of various concentrations of stock aqueous $I_3^-$ solution in a cuvette. We recorded the initial absorbance value with the help of UV−visible (UV−vis) spectroscopy. Then, 3 mg MOF was added to the cuvette. After treating the compound, we recorded the absorbance spectra of the supernatant solution at regular time intervals. We calculated the % removal data of $I_3^-$, the decrease in the concentration of the $I_3^-$ vs time, and the uptake of $I_3^-$ from this study using the following equations:

$$D_t = \frac{(C_0 - C_t)}{C_0} \times 100\% = \frac{(A_0 - A_t)}{A_0} \times 100\% \quad \text{..... (2)}$$

$$\frac{(C_0 - C_t)}{C_0} = \frac{(A_0 - A_t)}{A_0} \quad \text{..... (3)}$$

$$C_t = C_0 \times \left(1 - (A_0 - \frac{A_t}{A_0})\right) \quad \text{..... (4)}$$

$D_t$ is the exchange capacity, $C_0$ and $A_0$ are the initial concentration and absorbance of the $I_3^-$ solution, respectively, and $C_t$ and $A_t$ are the concentration and absorbance of the $I_3^-$ solution at specific times, respectively. The kinetics data were fitted to a pseudo-second-order kinetic model using the following equation.

**Pseudo-second-order model fitting:** To analyze the kinetic adsorption behavior towards triiodide, a pseudo-second-order kinetic model was used to evaluate the adsorption data, and its linear form can be expressed as follows:

$$t/Q_t = 1/Q_e^2 k_2 + t/Q_e \quad \text{..... (5)}$$

$$Q_t = \frac{Q_e^2 k_2 t}{(1 + Q_e k_2 t)} \quad \text{..... (6)}$$

Where Qt and Qe represent the adsorbed amount (mg/g) at time and at equilibrium t (min), respectively, $k_2$ represents the pseudo-second-order rate constant of adsorption (g $mg^{-1}$ $min^{-1}$). The experimental data was fitted using a pseudo-second-order kinetic model, and k2 is the correlation coefficient of the fitting curve.

**Uptake capacity studies:** 5 mg of MOFs were kept in contact with 5 mL of $I_3^-$ solutions bearing different concentrations (10000 to 50 ppm solution) for 24 h under stirring conditions. After 24 h, compounds were filtered out using a 0.22 μm syringe filter, and the filtrate was analyzed by UV−vis spectra. The absorbance was recorded by diluting the solution, and the final concentration was calculated from the initial and final absorbance values using equations (5). Finally, the uptake capacity was calculated using the following expression:

$$Q_t = (C_t - C_0)\frac{v}{m} \quad \text{..... (7)}$$

$Q_t$ is the uptake amount in mg/g, V is the volume of the solution in mL, and m is the mass of the compound in g.

Langmuir model: $Q_e = Q_m.C_e/(K_d+C_e)$, Where Ce(ppm) and Qe(mg g-1) are the I3− concentration at equilibrium and the amount of I3− adsorbed at equilibrium,

respectively. $Q_m$ (mg $g^{-1}$) is the maximum amount of $I_3^-$ per mass of adsorbent to form a complete monolayer. $K_d$ (mg $L^{-1}$) is a constant to the affinity of the binding sites.

**Selectivity test in the presence of other competing ions:** To examine the impact of competing ions, 5 mg of MOF was separately exposed to a binary solution consisting of 2.5 mL of $I_3^-$ solution and 2.5 mL of various competing anion solutions ($NO_3^-$, $Cl^-$, $Br^-$, $PO_4^{3-}$, $SO_4^{2-}$) in 100-fold excess concentration. The mixtures were stirred for 2 hours. After this period, the compounds were filtered out using a 0.22 µm syringe filter, and the filtrate was analyzed using UV-vis studies following the previously discussed protocol. The iodine uptake in the presence of a mixture of competing ions was also carried out using the same protocol.

**$I_3^-$ capture study in different water systems:** A stock solution of 100 ppm $I_3^-$ was prepared using various water matrices, including seawater, river water, lake water, etc. Next, 5 mg of MOF was added to 5 mL of these $I_3^-$ stock solutions and stirred for 2 hours. After the 2-hour period, the MOF was filtered out using a 0.22 µm syringe filter, and the filtrate was analyzed using UV-vis spectroscopy.

**Dynamic column-based flow-through $I_3^-$ capture study in water:** To check the continuous $I_3^-$ capture efficiency by iMOF-3C, a column exchange-based flow-through experiment was conducted by packing iMOF-3C inside a column as a bed, and Ravel Peristaltic Pump (Model No: RH-P110L-50) is used for flow rate control. After that, 100 ppm of $I_3^-$ aqueous solution passed through 100mg of iMOF-3C column bed with a flow rate of 1.5 ml/min. A bed volume of 10 mL of column eluted solution was collected in a different respective glass vial. Before and after capture studies, the concentration of $I_3^-$ solutions was analyzed by UV-vis spectroscopy.

## 2.4 Synthesis

### 2.4.1 Synthesis of Tris(4-(1H-imidazole-1-yl) phenyl)amineTIPA)ligand:

The TIPA ligand was synthesized with a reaction mixture of Tris(4-bromophenyl) amine (500 mg, 1.04 mmol), imidazole (460 mg, 6.75 mmol), $K_2CO_3$ (610 mg, 4.41 mmol), and anhydrous $CuSO_4$ (6.5 mg, 0.041mmol) was heated at 120 °C for 4-5 hours and then reaction was heated at 160-170 °C for 4.5 days under $N_2$ atmosphere. After that, the reaction was cooled down to room temperature, and washed with chloroform, THF, water, and methanol to remove unreacted product.(Scheme 1)[35]

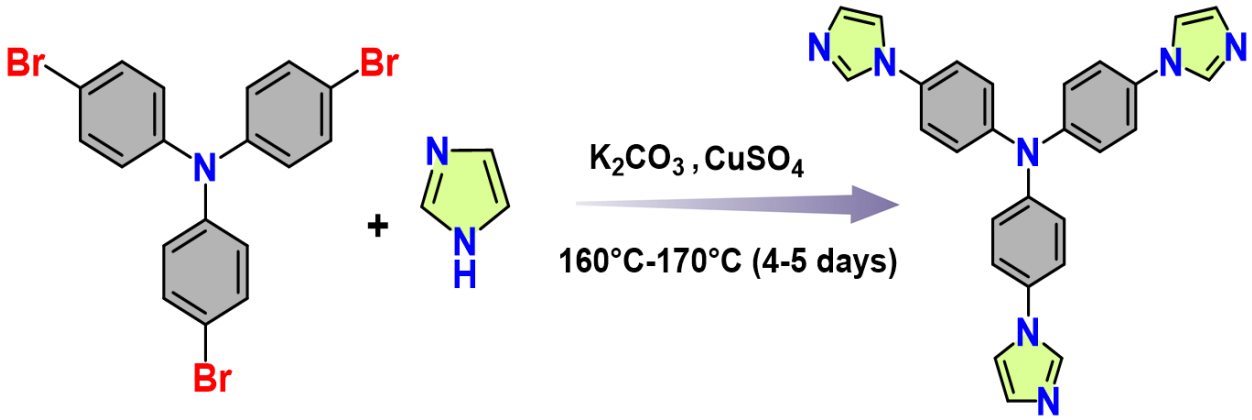


**Scheme-1:** Synthetic scheme of TIPA ligand

**2.4.2 Synthesis of iMOF-3C:** Single crystals of iMOF-3C were obtained in a solvothermal reaction at 130℃ from a mixture of $NiSO_4.xH_2O$ and ligand tris(4-(1H-imidazol-1-yl) phenyl) amine (TIPA) (1:1) in a solvent system of N, N-dimethylformamide (DMF) and water (2:1) (Scheme 2)[36].

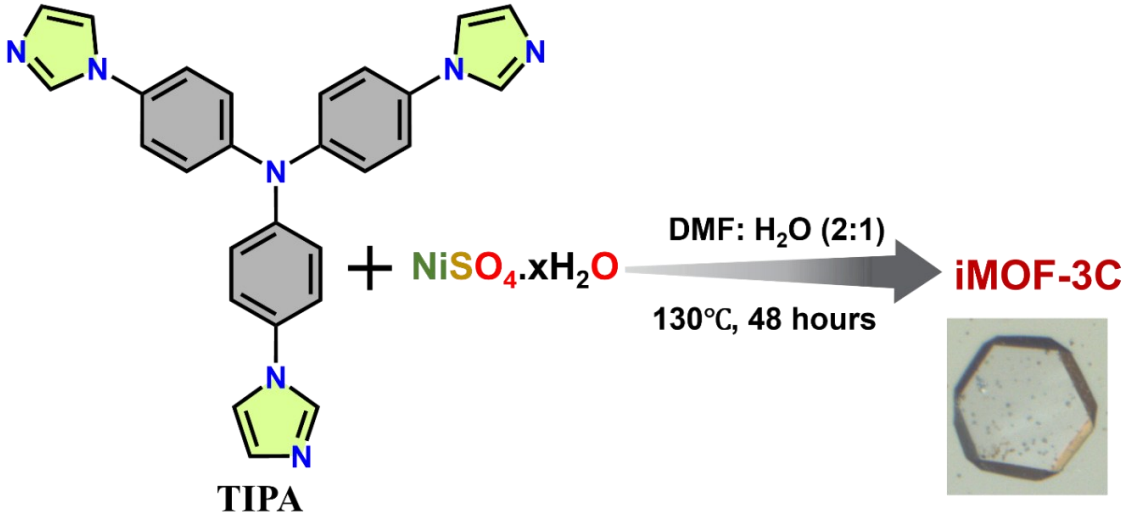


**Scheme-2:** Synthetic scheme of iMOF-3C (insert: digital images of IPM-200 crystal)

**2.4.3 Synthesis of IPM-201:** Single crystals of IPM-201 were obtained similarly, with the addition of BPSA in 1.5 times $NiSO_4.xH_2O$ in the reaction mixture (Scheme 3)[37].

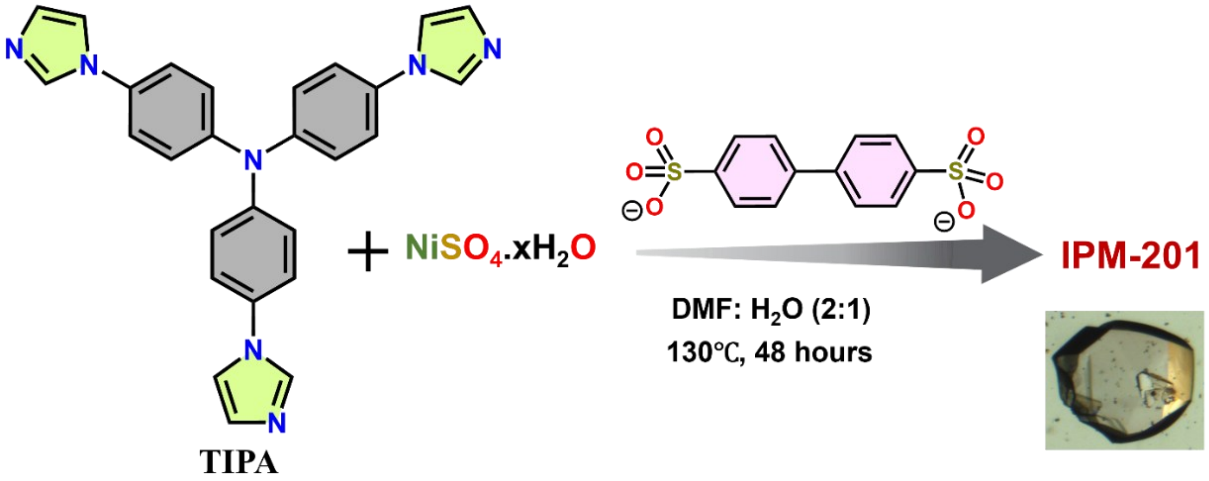


**Scheme-3:** Synthetic scheme of IPM-201 (insert: digital images of IPM-201 crystal)

# 3. Results and Discussion

## 3.1 Characterizations:

Both iMOF-3C and IPM-201 were isostructural; they crystallized in the R-3 space group, as revealed by single-crystal X-ray diffraction (SC-XRD) studies. The asymmetric unit (figure 3.1.a) is composed of one Ni(II) cation with 1/6 occupancy, one ligand (L) with 1/3 occupancy, and disordered solvent and organic anions. The metal center is octahedral, coordinating from six nitrogen atoms of six independent ligand units (figure 3.1.b). Detailed structure analysis shows that our iMOF-3C and IPM-201 show a two-dimensional layered structure. (figure 3.1.c). The crystal packing diagram depicts one-dimensional porous voids (figure 3.1.d). The pore dimensions of 6.6 x 4.89 Å were occupied by sulfate anions and biphenyl sulfonic acid, respectively[38].

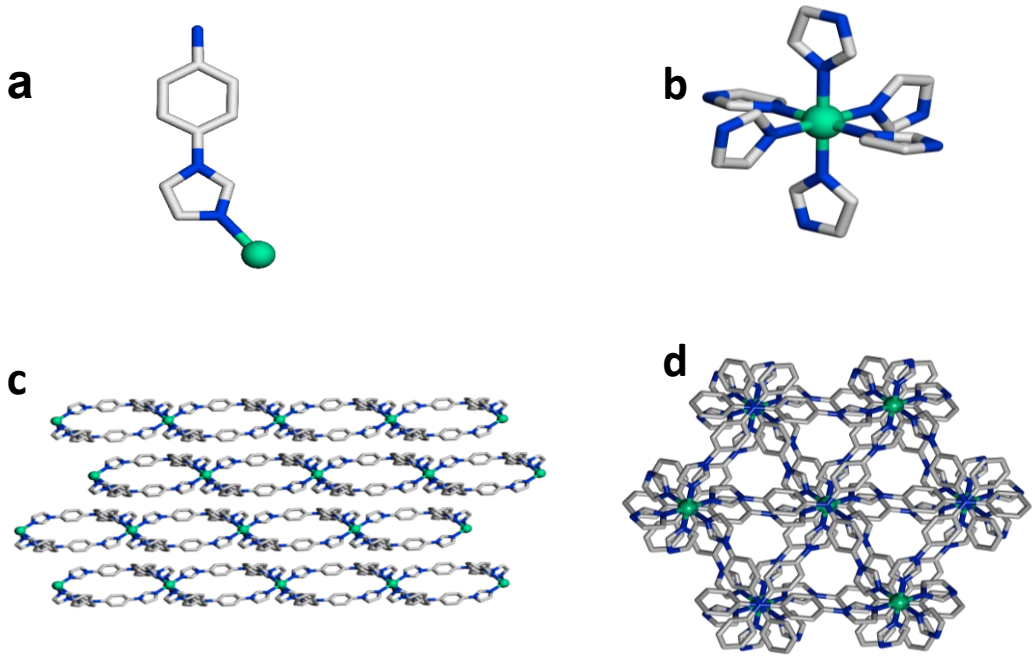


Figure 3.1 a.) asymmetric unit, b.) coordination environments, c.) layered structure, and d.) crystal packing unit.

---

Synthesized iMOF-3C and IPM-201 were further characterized by various techniques such as Powder X-ray diffraction (PXRD), Thermogravimetric Analysis (TGA), Fourier Transform Infrared spectra (FT-IR), $CO_2$ at 195K adsorption-desorption isotherm, Field Emission Scanning Electron Microscopy (FESEM) and X-ray photoelectron spectroscopy (XPS), etc.

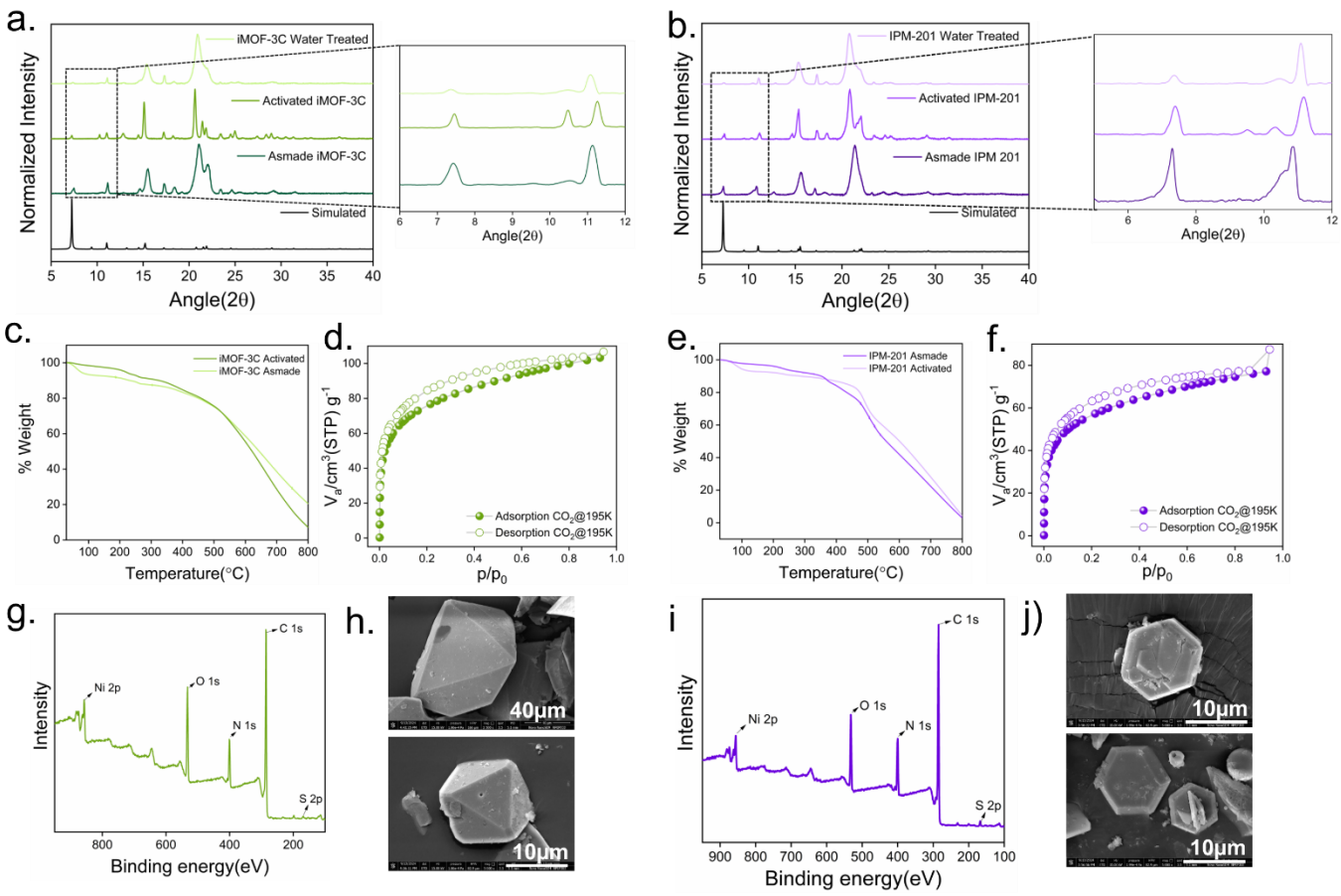


Figure 3.2.: a. PXRD profile of iMOF-3C, b. IPM-201(along with zoom views to show the peaks well matched with simulated structure) c. TGA of iMOF-3C d. $CO_2$@195K adsorption-desorption isotherm of iMOF-3C e. TGA of IPM-201 f. $CO_2$@195K adsorption-desorption isotherm of IPM-201 g. XPS survey spectra of iMOF-3C h. FESEM images of iMOF-3C i. XPS survey spectra of IPM-201 j. FESEM images of IPM-201.

The bulk phase purity of both the MOFs was assessed by PXRD analysis, which revealed that the diffraction patterns of both MOFs in their as-synthesized, activated states and after water treatment matched well with the simulated pattern of the pristine MOFs (figure 3.2 a, b). The TGA profiles of both as-synthesized MOFs, iMOF-3C and IPM-201, exhibit an initial weight loss due to the release of guest molecules, water, and DMF. In contrast, after guest removal, the activated MOFs display no initial weight loss and demonstrate high thermal stability up to ~450°C. (figure 3.2 b, e). FT-IR analysis reveals characteristic peaks at 1070 $cm^{-1}$ and 1134 $cm^{-1}$ corresponding to sulfur in the form of $SO_4^{2-}$, indicating successful incorporation of sulfate counter anions in iMOF-3C. Similarly, the FT-IR analysis of IPM-201 reveals corresponding stretching frequency at 1032 $cm^{-1}$ and 1193 $cm^{-1}$ corresponds to the sulphonic acid's groups of

BPSA, along with the well-matched peak of monomer in MOFs, confirming the formation of IPM-201. (Appendix A1, Appendix A2). X-ray photoelectron spectroscopy (XPS) was utilized to systematically analyze the electronic structure of the MOFs. The survey scan of iMOF-3C exhibited five distinct peaks at approximately 857.14 eV, 531.64 eV, 400.75 eV, 286.23 eV, and 168.71 eV, corresponding to the binding energies of Nickel (Ni), Oxygen (O), Nitrogen (N), Carbon (C), and Sulfur (S), respectively. Notably, IPM-201 displayed nearly identical binding energy values to those of iMOF-3C owing to their isostructural property (figure 3.2 g, i). Further, FESEM analysis reveals that both MOFs have hexagonal morphology (figure 3.2 g, j)

## 3.2 Iodine Capture Study:

Following the successful synthesis and characterization of the MOFs, their iodine sequestration capabilities were systematically investigated. Given the substantial environmental hazard posed by iodine in its vapor phase, an initial adsorption study was conducted under these conditions. The iodine uptake performance of iMOF-3C and IPM-201 was evaluated using a standard gravimetric method. To mimic the conditions relevant to nuclear fuel reprocessing, iodine vapor sequestration experiments were carried out at 75°C. Upon exposure to iodine vapor, both IPM-201 and iMOF-3C exhibited a distinct color change to a darker hue, suggesting efficient adsorption within the porous framework of the MOFs. Kinetic studies revealed that the equilibrium adsorption capacities of IPM-201 and iMOF-3C reached 4.44 and 4.21 $g \cdot g^{-1}$, respectively, after 48 hours (figure 3.3 c). Additionally, considering the high volatility of $I_2$, adsorption studies were also performed at ambient temperature. Under these conditions, the equilibrium uptake capacities for IPM-201 and iMOF-3C were determined to be 0.486 and 0.515 $g \cdot g^{-1}$, respectively, after 24 hours (figure 3.3 d).

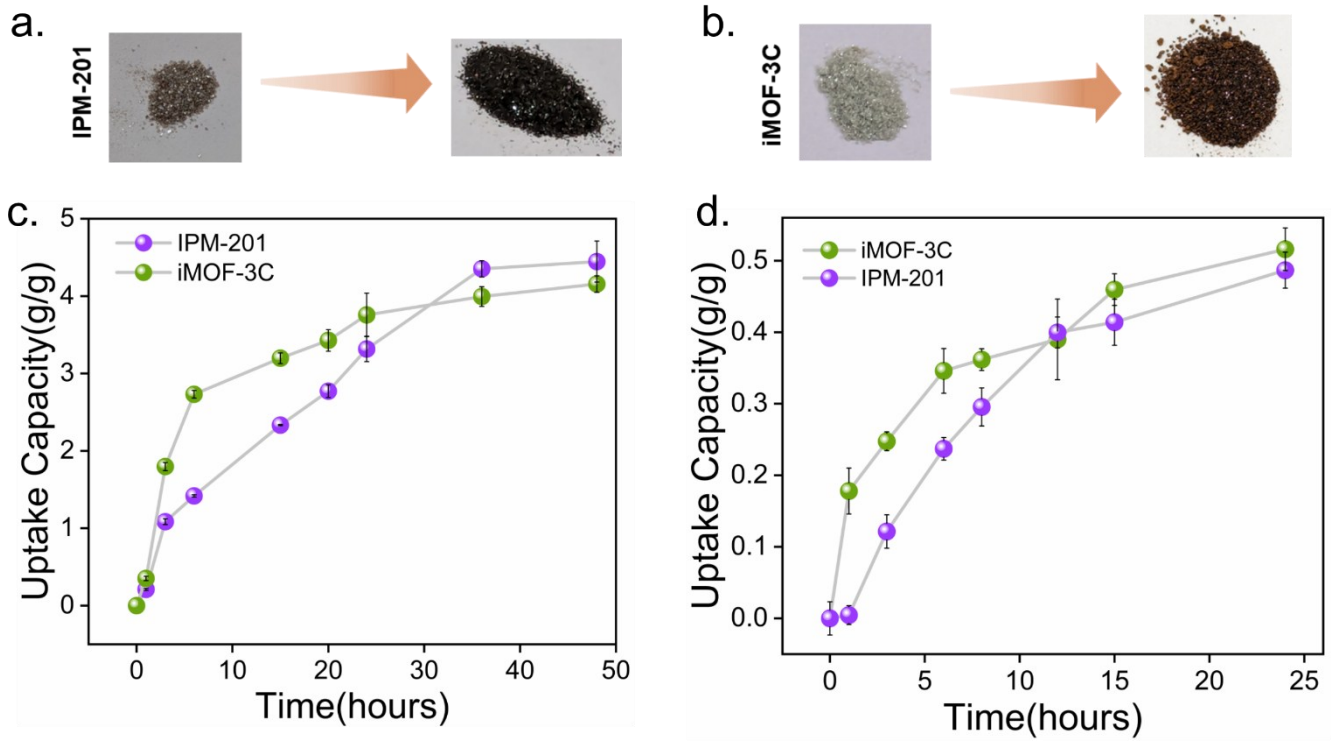


Figure 3.3. Digital images of before and after iodine vapor adsorption of a. IPM-201 b. iMOF-3C at 75°C. c. Gaseous iodine uptake capacities of both MOFs at 75°C in static condition d. Gaseous iodine uptake capacities of both MOFs at room temperature in static conditions.

The efficient and selective extraction of iodine species from aqueous media is paramount for real-time water treatment applications. Considering the cationic nature of the MOFs, with free counter-anions BPSA in IPM-201 and $SO_4^{2-}$ in iMOF-3C, their ability to sequester iodide species (e.g., $I_3^-$) was systematically investigated using an aqueous solution of KI and $I_2$. For initial observation, the adsorption kinetics were monitored via UV–Vis spectroscopy by tracking the absorbance maxima ($\lambda_{max}$) at 350 nm over time. Notably, IPM-201 exhibited rapid adsorption, removing >99% of $I_3^-$ within 10 minutes (figure 3.4 b.). In contrast, iMOF-3C displayed even faster kinetics, achieving >99% removal within 30 seconds from a 50 ppm $I_3^-$ solution, underscoring its exceptional affinity for iodide species (figure 3.4 c.). Kinetic modeling revealed that the adsorption process adheres to a pseudo-second-order mechanism, as demonstrated by a non-linear fit of adsorption capacity ($Q_t$) versus time (t), yielding an excellent correlation coefficient ($R^2 \approx 0.999$) for both MOFs (figure 3.4 d, Appendix A3-Appendix A3). The rate constants, obtained from the linear fit of the pseudo-second-order model, were determined to be $1.344 \times 10^{-3}$ and $4.481 \times 10^{-3}$ $g.mg^{-1}.sec^{-1}$ for IPM-201 and iMOF-3C, respectively, further confirming the rapid adsorption kinetics. Despite both MOFs exhibiting fast uptake, iMOF-3C consistently demonstrated

superior kinetics. To validate these observations, kinetic experiments were performed at higher initial concentrations (100 ppm and 200 ppm), revealing similar trends and reinforcing the enhanced adsorption kinetics of iMOF-3C (Appendix(A5-A6)). The pronounced difference in adsorption rates is attributed to the nature of the counter-anions present in the MOFs. It is hypothesized that the $SO_4^{2-}$ anions in iMOF-3C facilitate a more efficient ion-exchange process with $I_3^-$ compared to BPSA in IPM-201, thereby accelerating the adsorption kinetics. Equilibrium adsorption studies further supported this hypothesis, as the concentration-dependent uptake capacities of $I_3^-$ were well-described by the Langmuir isotherm model, yielding maximum iodine sorption capacities of 2.54 and 3.28 $g \cdot g^{-1}$ for IPM-201 and iMOF-3C, respectively (figure 3.4 e.) Further substantiating the superior ion-exchange efficiency of $SO_4^{2-}$ over BPSA in $I_3^-$ sequestration. Given that real-world aqueous systems contain various competing ions at high concentrations, diverse pH conditions, and different water matrices, the selective sequestration of $I_3^-$ by both MOFs was systematically evaluated under these conditions. First, the sorption selectivity of IPM-201 and iMOF-3C was investigated in the presence of competing anions ($SO_4^{2-}$, $Br^-$, $Cl^-$, $NO_3^-$, $HPO_4^{2-}$) at 100-fold excess concentration relative to $KI/I_2$ (figure 3.4 g.). Despite the presence of these competing species, iMOF-3C exhibited significantly faster $I_3^-$ removal than IPM-201, as evidenced by its UV–Vis spectra (Appendix A9-A10). Although at equilibrium, both MOFs reach a removal efficiency of >99%. To further investigate the influence of solution pH on $I_3^-$ removal, adsorption experiments were conducted over a pH range of 4–10. Across all tested conditions, iMOF-3C consistently exhibited faster kinetics than IPM-201, ultimately achieving near-complete removal of $I_3^-$ at equilibrium for both MOFs (Figure 3.4 h, Appendix A11, Appendix A12). Encouraged by these findings, we extended the sequestration studies to different water matrices, including seawater, lake water, and tap water, to assess performance under complex ionic environments. Both MOFs demonstrated robust and efficient removal across all water types, with iMOF-3C consistently displaying superior adsorption kinetics (Figure 3.4 i, Appendix A13, Appendix A14.). The enhanced performance of iMOF-3C is attributed to the nature of its counter-anion, $SO_4^{2-}$, which possesses higher hydration energy compared to the organic BPSA anion in IPM-201. This increased hydration energy likely facilitates a more rapid and efficient anion-exchange process, wherein $I_3^-$ readily

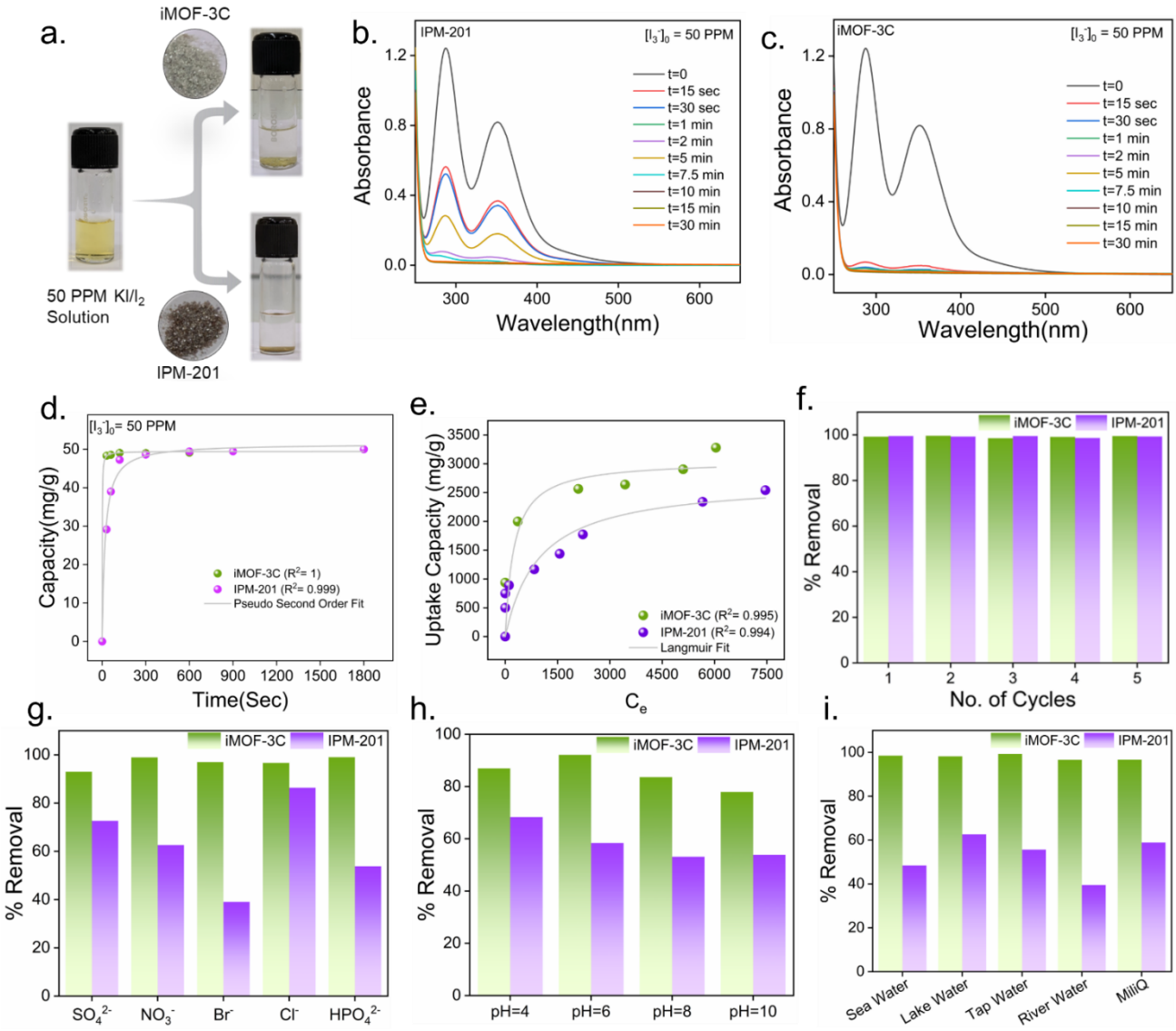


Figure 3.4. a. Schematic optical images of kinetics process. UV/Vis spectra of $I_3^-$ as a function of time in the presence of b. IPM-201 c. iMOF-3C d. Non-linear pseudo-second order fit f. Recyclability test g. percentage removal against various competing ions after 30 seconds h. percentage removal against pH variation after 30 seconds. i. percentage removal against various water matrixes after 30 seconds.

displaces $SO_4^{2-}$. Additionally, in IPM-201, the presence of aromatic π-rings may contribute to metal-π and π-π interactions, potentially impeding the diffusion and exchange kinetics of $I_3^-$. Despite this, IPM-201 still exhibited high removal efficiency, underscoring the dominance of ion exchange as the primary sequestration mechanism in both MOFs. The long-term viability of these materials was further evaluated through recyclability studies, as retention of adsorption efficiency over multiple cycles is a critical parameter for practical deployment. Both MOFs exhibited exceptional stability,

with negligible loss in removal efficiency over five consecutive adsorption-desorption cycles, highlighting their potential for sustainable and effective iodine remediation applications (Figure 3.4 f).

To further exploit the exceptional kinetics and high efficiency of iMOF-3C in triiodide ($I_3^-$) sequestration, its performance was evaluated under dynamic column-based flow conditions for continuous aqueous-phase iodine capture. A packed-bed column was prepared by loading iMOF-3C, and an aqueous $I_3^-$ solution was continuously passed through the system (Figure 3.5a). The initial yellow-colored solution was progressively decolorized upon elution, indicating efficient adsorption of triiodide species. Quantitative analysis via UV–Vis spectroscopy of the first dynamic breakthrough cycle

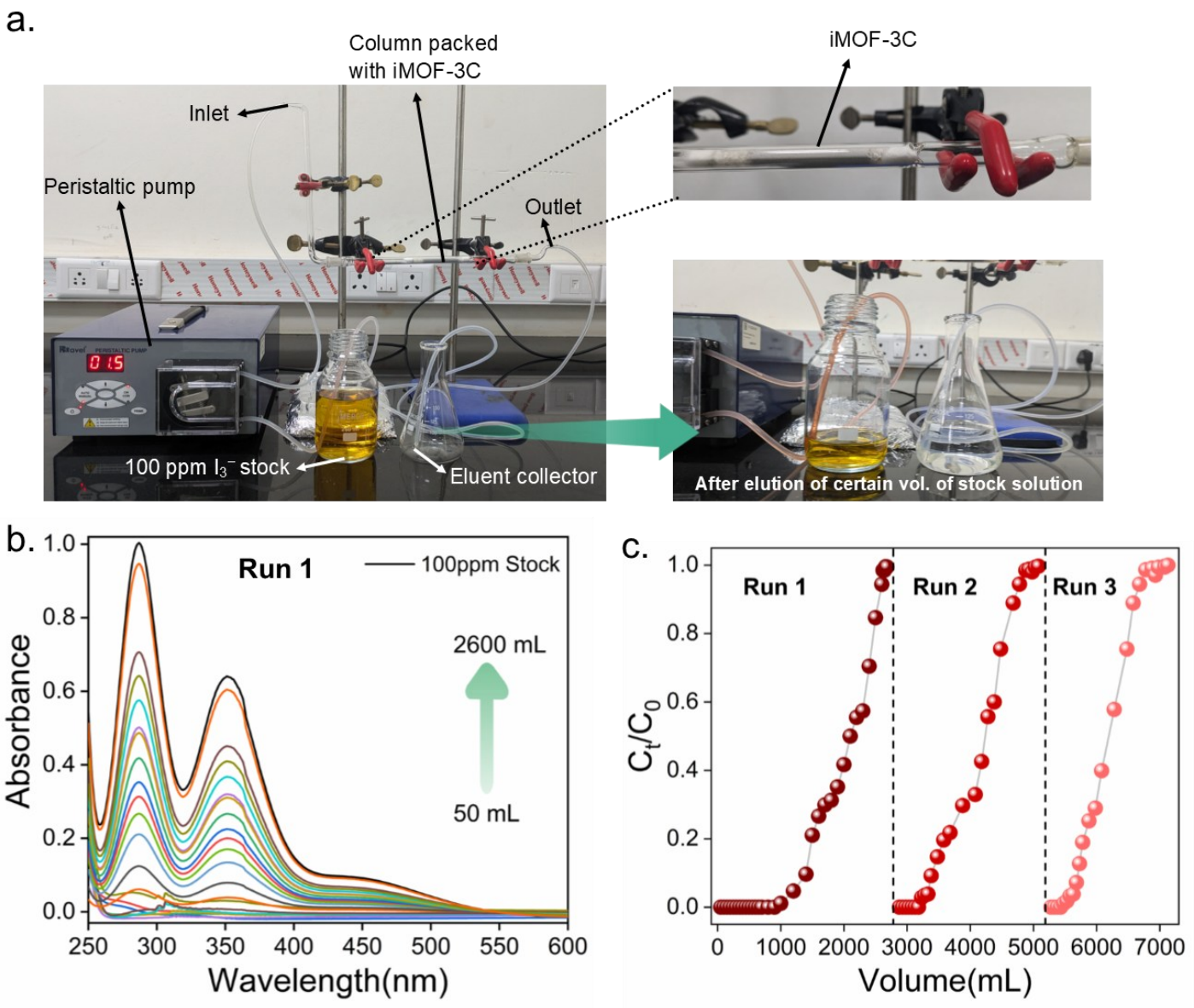


Figure 3.5 a. Digital photographs of dynamic column breakthrough setup b. UV-vis profile of run 1 c. Breakthrough profile of column-based I2/KI capture test

revealed that the column effectively processed approximately 1100 mL of a 100 ppm $I_3^-$ solution with ~99% removal efficiency, ultimately achieving a cumulative treatment volume of ~2600 mL before reaching saturation upon the passing of ~2600mL of 100 ppm $I_3^-$ solutions (Figure 3.5b). The column was regenerated by treating it with an excess concentration of $Na_2SO_4$ solution, followed by subsequent adsorption cycles. Notably, iMOF-3C retained its high removal efficiency over three successive cycles, demonstrating its structural stability and recyclability under continuous flow conditions (Figure 3.5c). These results underscore the strong potential of iMOF-3C as a highly efficient and regenerable adsorbent for dynamic aqueous-phase iodine sequestration, further establishing its applicability in real-world iodine remediation strategies.

## 3.3 Mechanistic Insights:

Building on the remarkable iodine removal performance of both MOFs, we explored the adsorption mechanism through a series of experiments conducted on $I_3^-$@iMOF-3C and $I_3^-$@IPM-201. The optical microscopy analysis of iodide-loaded single crystals of both IPM-201 and iMOF-3C initially revealed a pronounced dark coloration, confirming the successful encapsulation of iodine within the MOF framework (Figure 3.6a). FESEM images reveal that the morphological integrity of both MOFs remains nearly unaltered post-adsorption, underscoring their high structural stability (Figure 3.6c, Appendix A15). Additionally, FESEM-EDX elemental mapping confirms a homogenous spatial distribution of iodine across the MOF frameworks (Table T1, T2). To elucidate the chemical state and binding interactions of the immobilized iodine species, X-ray photoelectron spectroscopy (XPS) was employed. The survey XPS spectra of $I_3^-$@iMOF-3C and $I_3^-$@IPM-201 exhibit characteristic iodine signals corresponding to the $I_3^-$ (Figure 3.6 b.). Deconvolution of the I 3d XPS spectra for both MOFs reveals two intense peaks at 619.2 eV and 630.8 eV, corresponding to polyiodide ($I_3^-$), specifically the I $3d_{5/2}$ and I $3d_{3/2}$ orbitals. Furthermore, the Ni 2p XPS spectra of iMOF-3C display a binding energy shift to lower energy, indicative of electronic interactions between the nickel sites and the adsorbed iodide anions (Appendix A16, A17). This shift suggests a successful anion-exchange process wherein $I_3$ replaces $SO_4^{2-}$ ions$^-$. A similar trend is observed in the Ni 2p XPS spectra of IPM-201. Post-adsorption, the N 1s, and C 1s XPS spectra exhibit negligible variations, suggesting

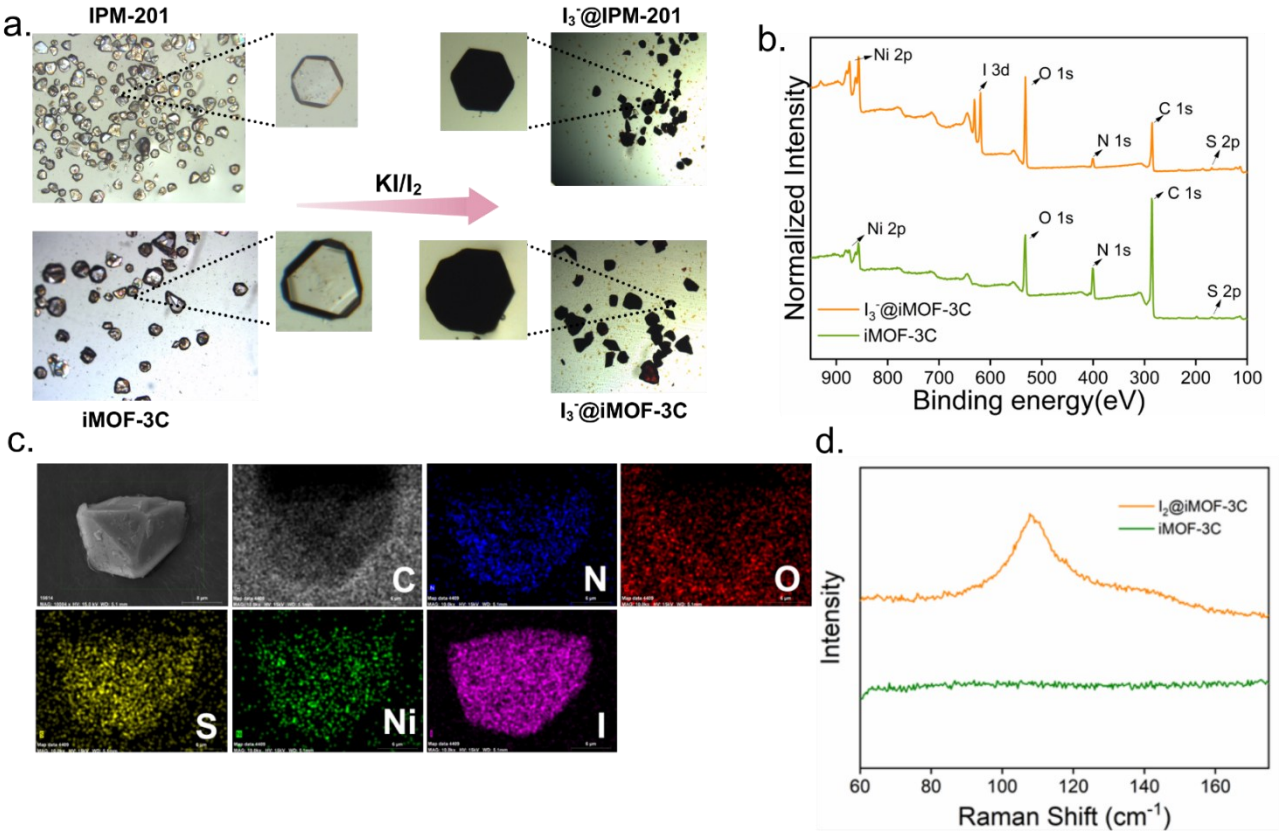


Figure 3.6 a. Optical microscopy images of before and after $I_3^-$ capture by MOFs b. XPS survey spectra of iMOF-3C and $I_3^-$@iMOF-3C c. FESEM EDX mapping of iMOF-3C post $I_3^-$ capture. d. Raman spectra of $I_3^-$@iMOF-3C.

that the ligand framework does not participate directly in iodide adsorption. Raman spectroscopy provides additional insight into the adsorption process, with pristine MOFs exhibiting no significant Raman-active features, whereas iodide-loaded $I_3^-$@iMOF-3C and $I_3^-$@IPM-201 display a distinct broad peak at ~110 $cm^{-1}$, characteristic of $I_3^-$ stretching vibrations (Figure 3.6 d, Appendix A18). Furthermore, solid-state UV-Vis spectroscopy was conducted on both pristine and iodide-loaded MOFs to probe electronic transitions associated with iodide incorporation. The UV spectra of $I_3^-$@iMOF-3C and $I_3^-$@IPM-201 exhibit distinct shoulder peaks at wavelength 410 nm, arising from iodide-related electronic transitions, providing further confirmation of successful iodide encapsulation within the MOF matrices (Appendix A19, Appendix A20). The PXRD patterns of $I_3^-$@iMOF-3C and $I_3^-$@IPM-201 exhibit the absence of discernible diffraction peaks in the lower-angle region, suggesting structural modifications following iodide incorporation (Appendix A21, Appendix A22). Thermogravimetric analysis (TGA) of $I_3^-$@iMOF-3C indicates that polyiodide loading does not induce significant structural degradation; however, a minor yet consistent

weight loss is observed across the thermal range, attributable to the presence of weakly bound iodide species within the MOF pores (Appendix A23). A similar thermal stability trend is observed for $I_3^-$@IPM-201, as reflected in its TGA profile (Appendix A24). Elemental analysis was conducted on pristine and iodide-loaded MOFs to investigate further and validate the anion exchange process. For IPM-201, the atomic sulfur content (%S) decreases from 3.30% in the pristine framework to 2.31% post $I_3^-$ adsorption, indicating the partial displacement of BPSA anions by polyiodide species (Table T3). In the case of iMOF-3C, the %S content reduces from 1.03% to 0.522% upon $I_3^-$ loading, further validating the successful exchange of $SO_4^{2-}$ with $I_3^-$ anions within the framework (TableT3).

## 4. Conclusion:

In conclusion, we have strategically designed and synthesized two isostructural ionic metal-organic frameworks (iMOF-3C and IPM-201) featuring $SO_4^{2-}$ and BPSA as counter anions, respectively. Detailed crystallographic analysis and comprehensive physicochemical characterizations were performed to elucidate their structural and functional attributes. The primary objective of this study was to achieve efficient iodine sequestration. Both MOFs demonstrated exceptional iodine uptake from the vapor phase at 75°C as well as under ambient conditions. Encouraged by these findings, we further investigated their efficacy in triiodide ($I_3^-$) sequestration from aqueous media. As anticipated, both frameworks exhibited rapid adsorption kinetics and high uptake capacities, with iMOF-3C displaying enhanced kinetics relative to IPM-201. This superior performance is attributed to the presence of $SO_4^{2-}$, which facilitates more efficient ion exchange with $I_3^-$. Furthermore, the robustness and practical applicability of these MOFs were evaluated under various real-world conditions, including complex water matrices, competing ionic species, and diverse pH environments. Notably, both frameworks exhibited excellent recyclability, underscoring their potential as efficient and sustainable adsorbents for iodine sequestration from both aqueous and gaseous phases.

# 5. APPENDIX

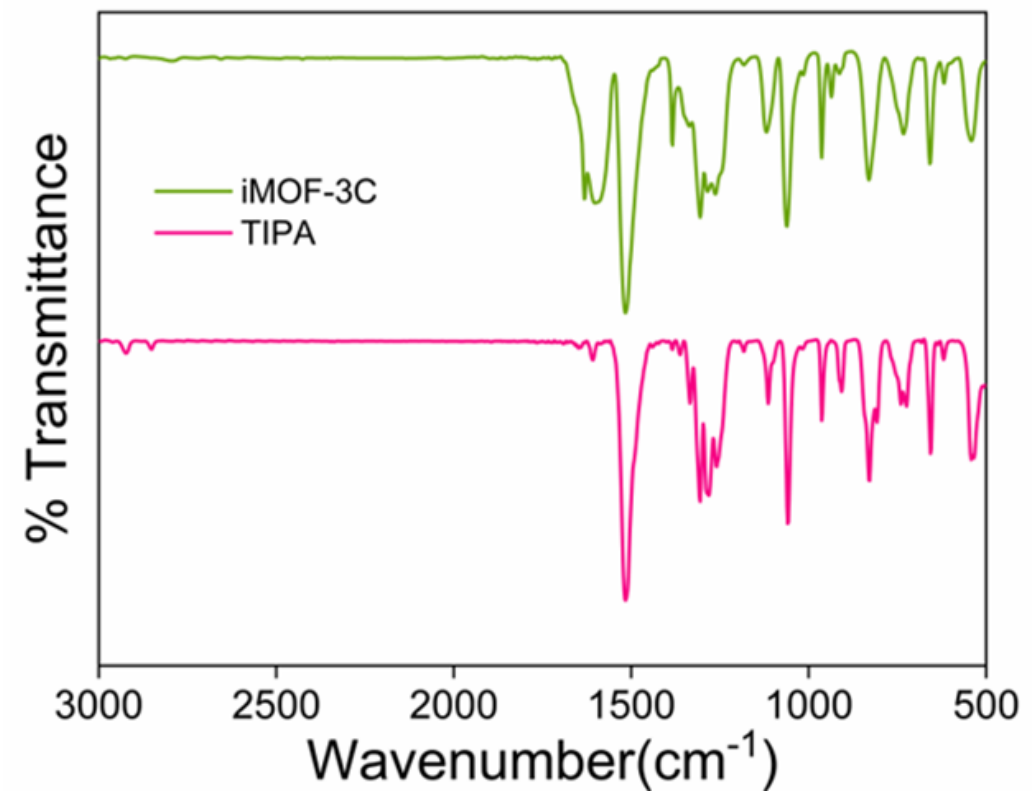


Appendix A1: FT-IR spectra of pristine iMOF-3C

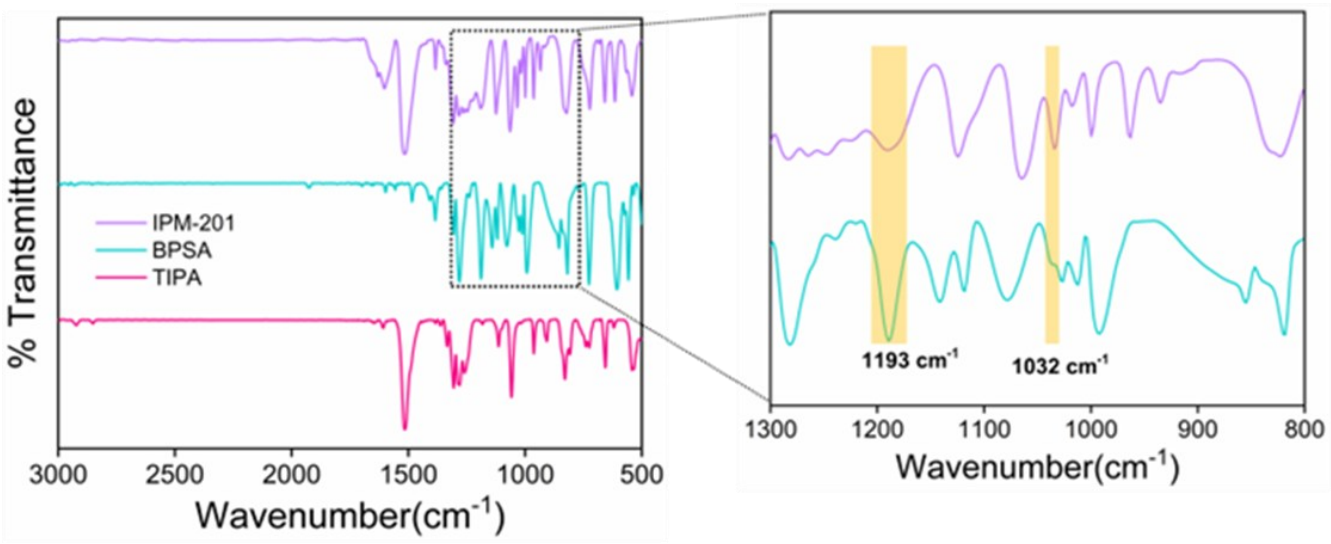


Appendix A2: FT-IR spectra of pristine IPM-201 showing the corresponding peak of sulphonic acid

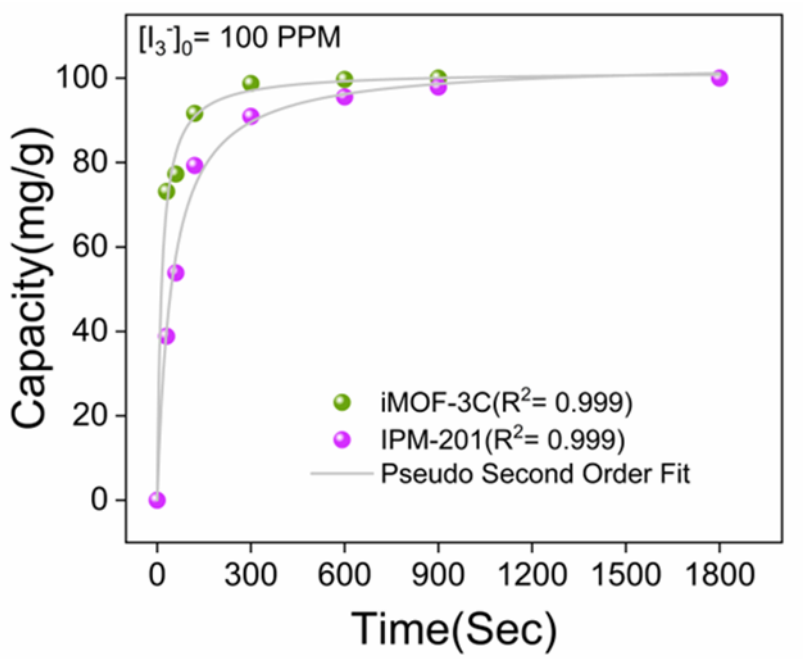


Appendix A3: Non-linear pseudo-second order fit with an initial concentration of $I_3^-$ 100 ppm

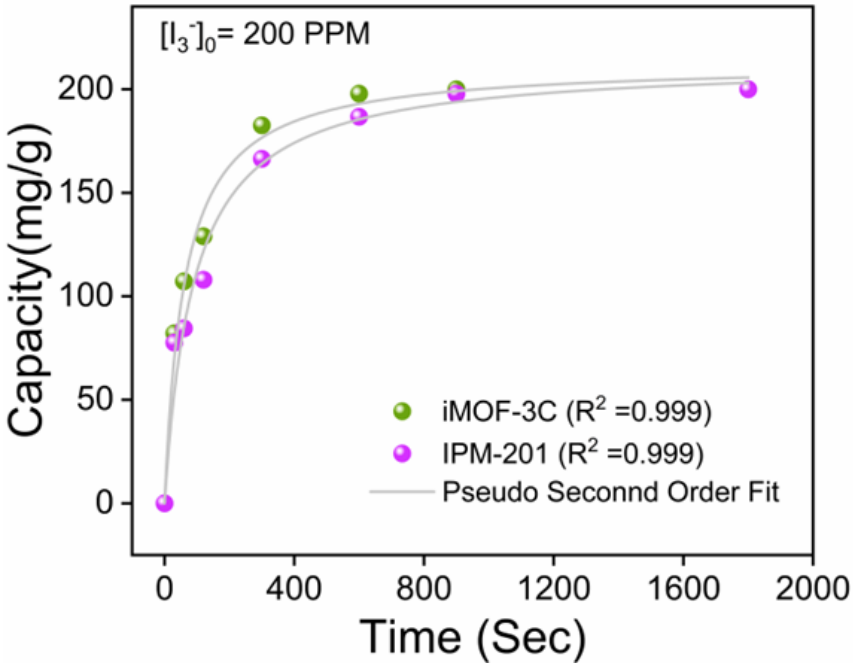


Appendix A4: Non-linear pseudo-second order fit with an initial concentration of $I_3^-$ 100 ppm

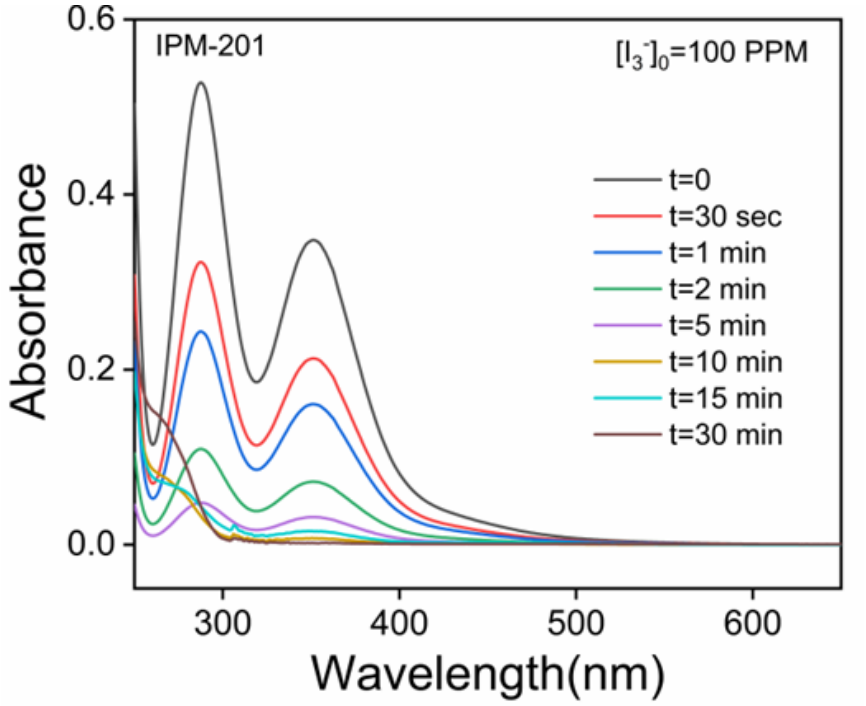


Appendix A5: Kinetic profiles of IPM-201 towards of $I_3^-$ at100 ppm

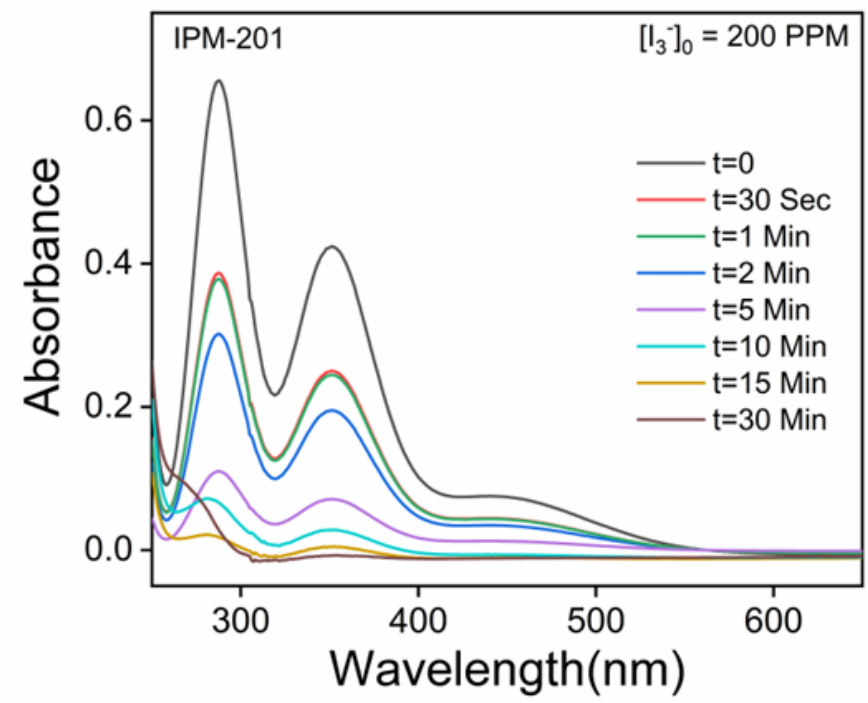


Appendix A6: Kinetic profiles of IPM-201 towards $I_3^-$ at 200 ppm

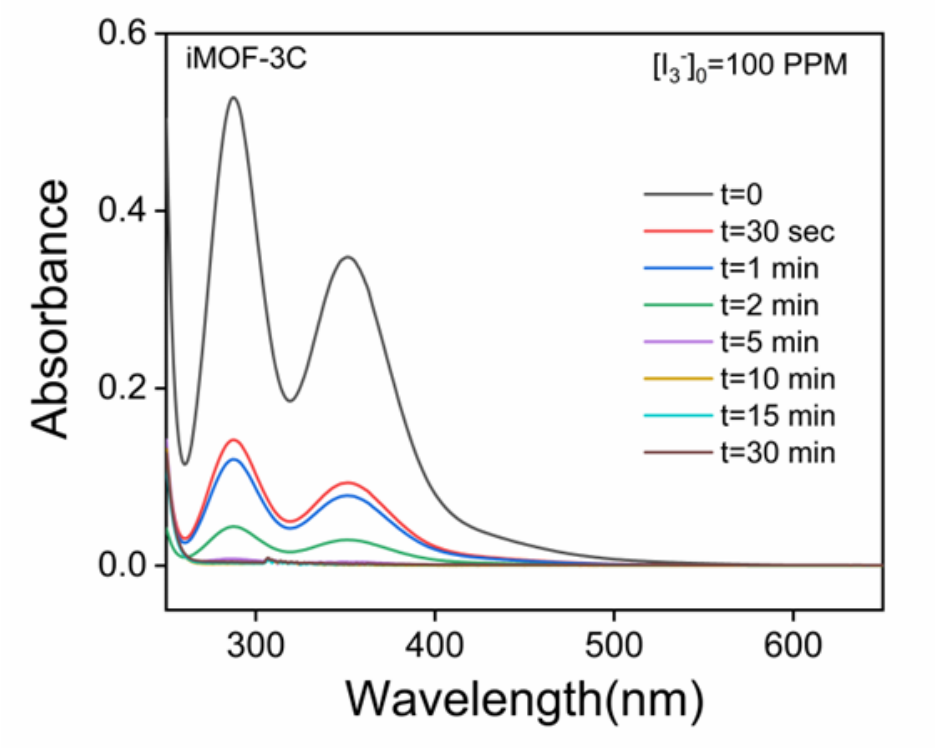


Appendix A7: Kinetic profiles of iMOF-3C towards $I_3^-$ at 100 ppm

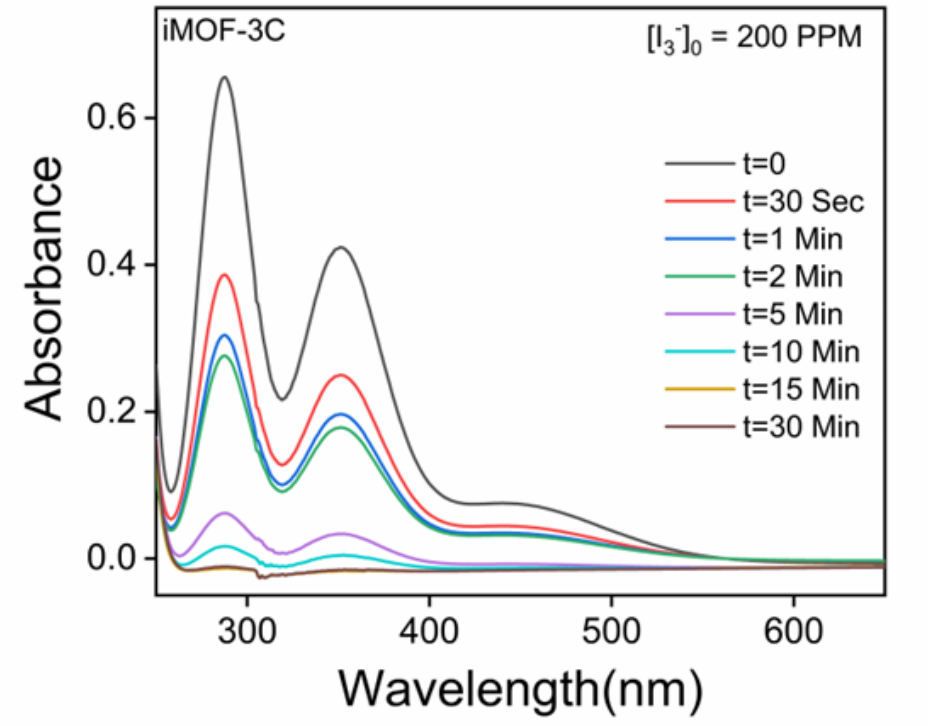


Appendix A8: Kinetic profiles of iMOF-3C towards of $I_3^-$ at 200 ppm

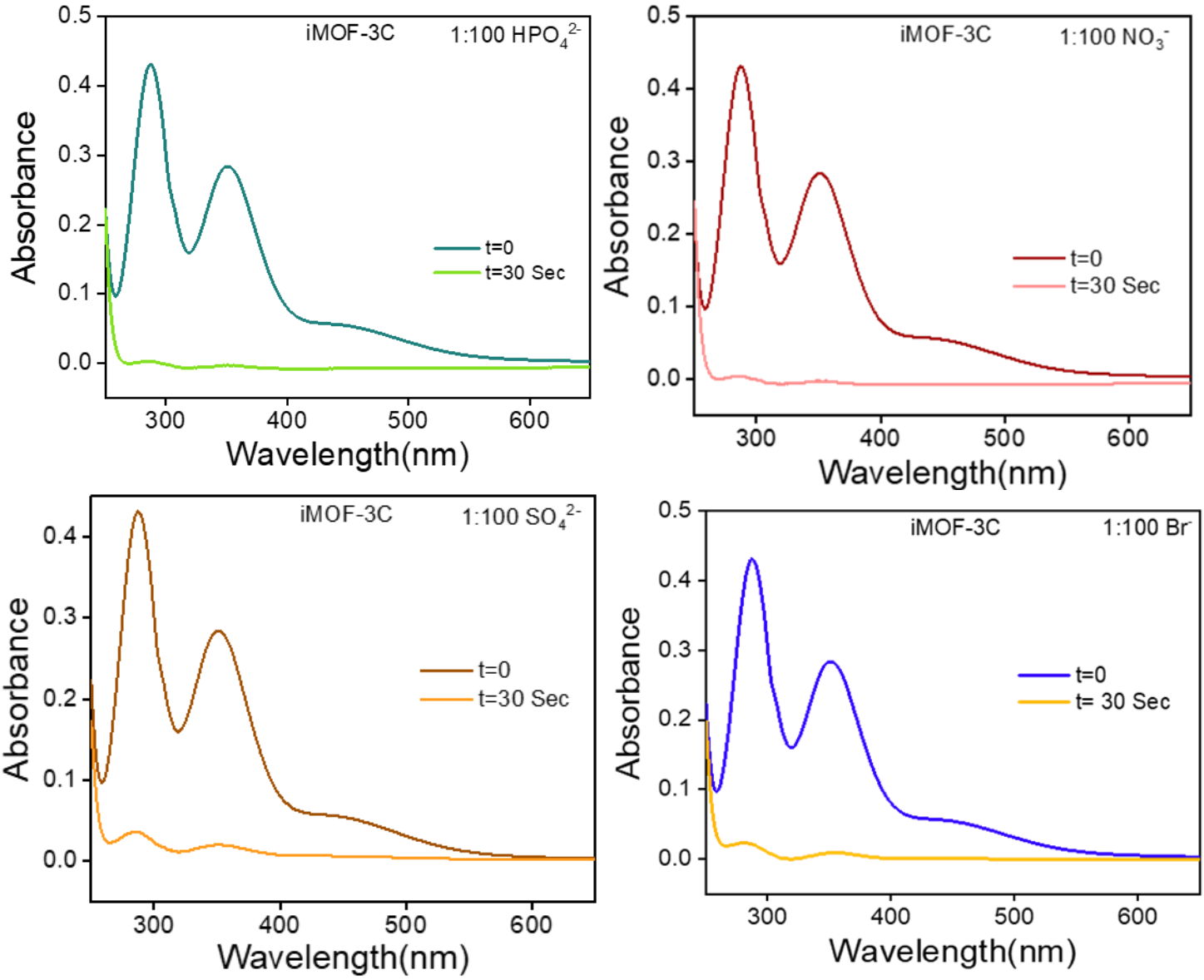


Appendix A9: Time-dependent UV-vis spectra of $I_3^-$ in the presence of different competing ions treated with iMOF-3C

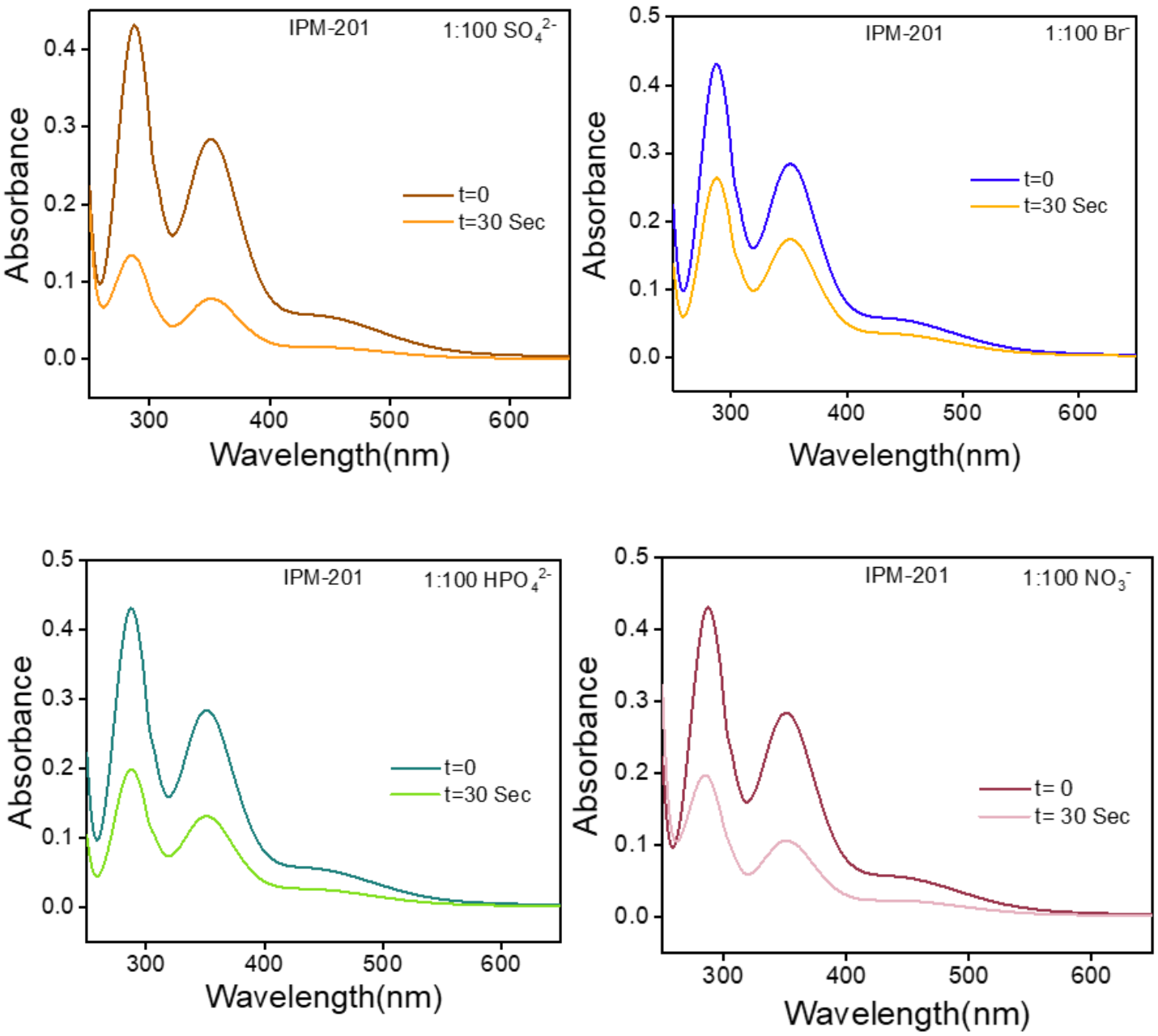


Appendix A10: Time-dependent UV-vis spectra of $I_3^-$ in the presence of different competing ions treated with IPM-201

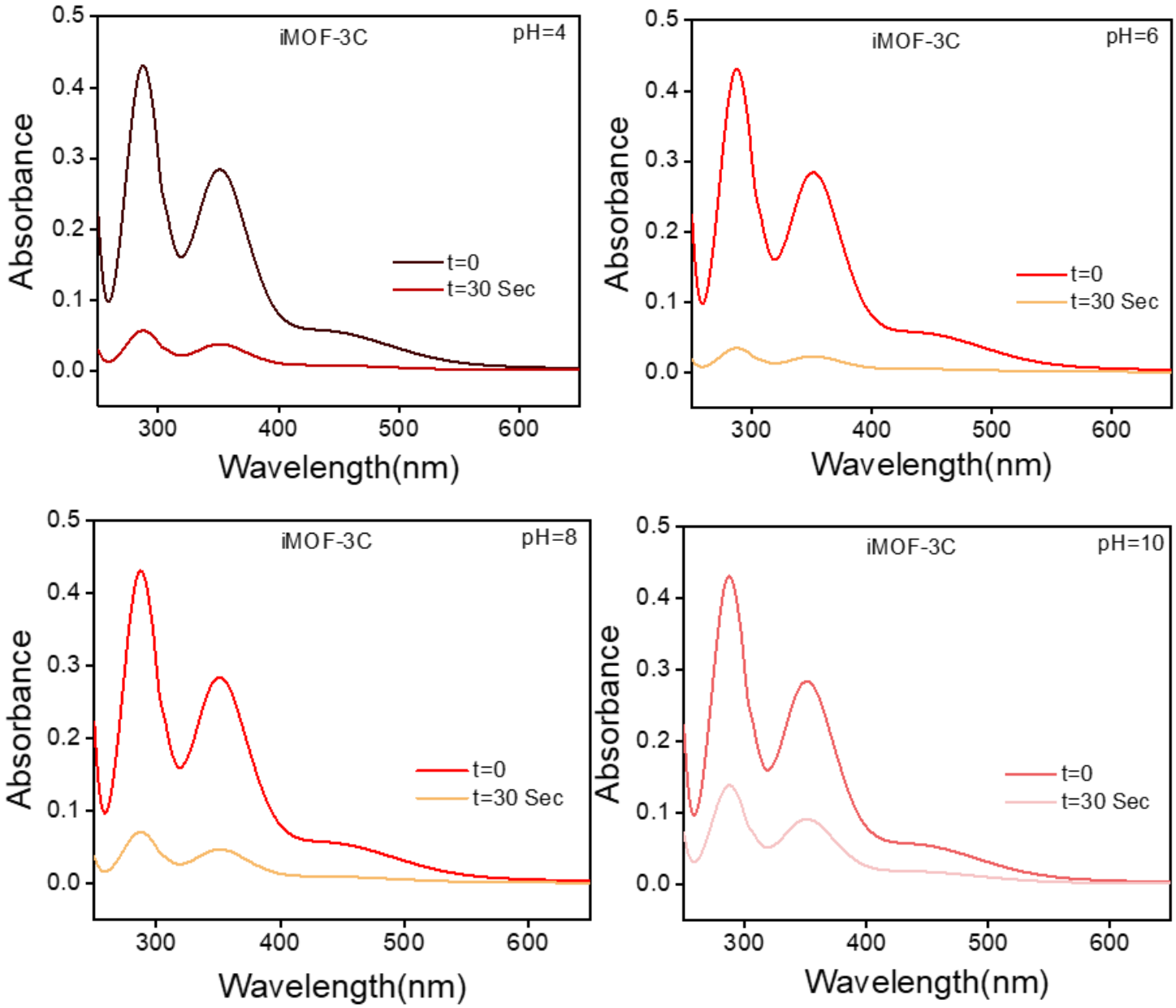


Appendix A11: Time-dependent UV-vis spectra of $I_3^-$ in different pH conditions treated with iMOF-3C

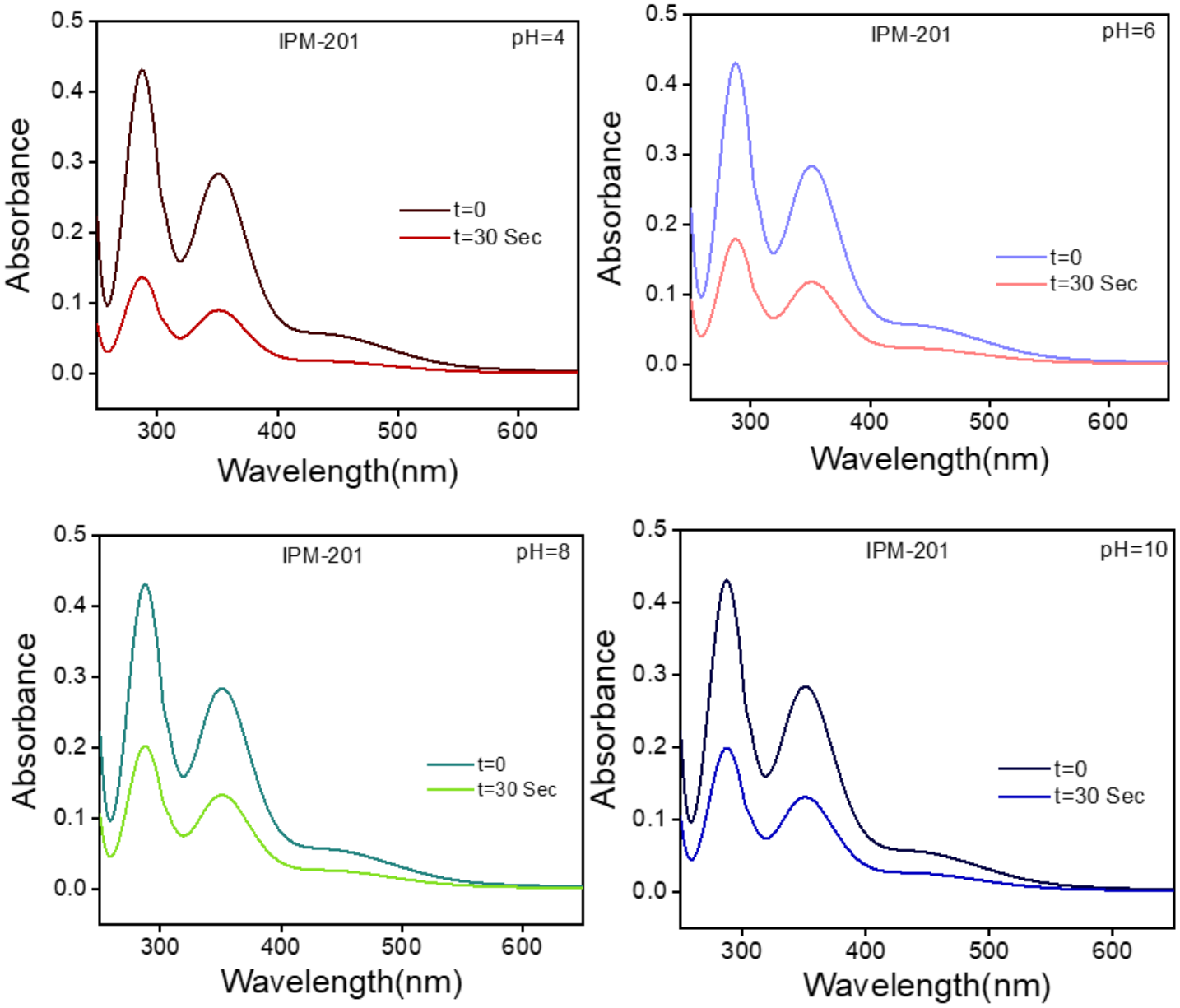


Appendix A12: Time-dependent UV-vis spectra of $I_3^-$ in different pH conditions treated with IPM-201

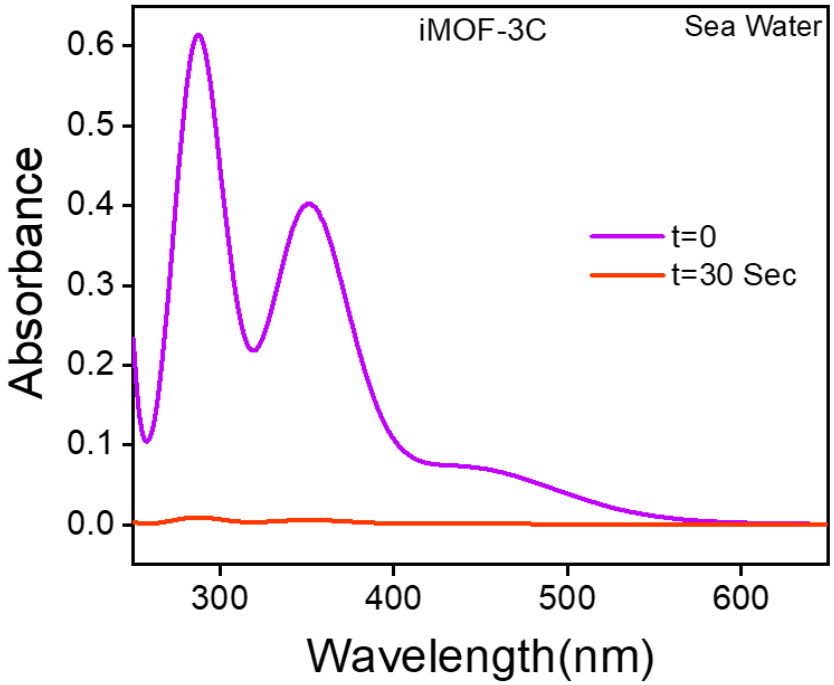


Appendix A13: Time-dependent Uv-vis spectra of $I_3^-$ in seawater showing rapid dismissing by the treatment of iMOF-3C

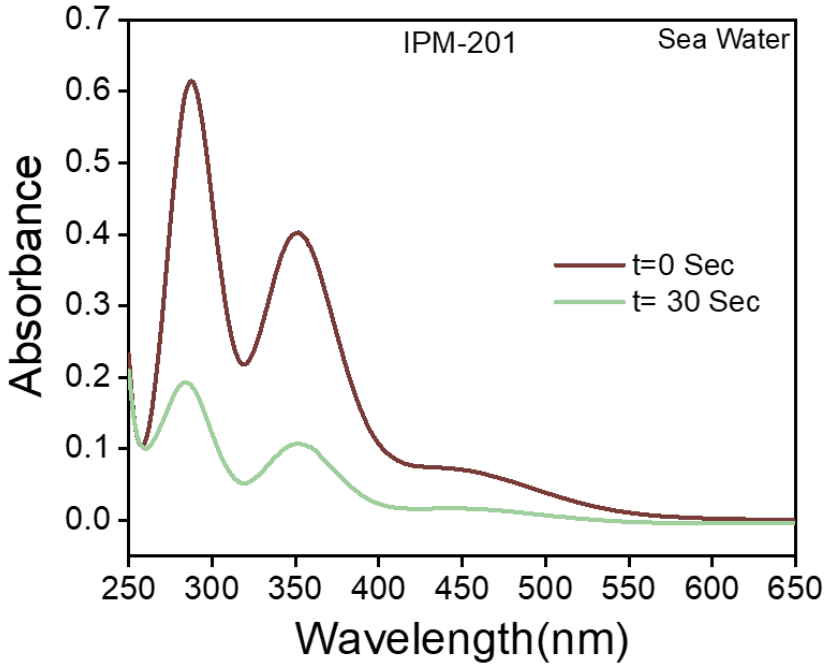


Appendix A14: Time-dependent Uv-vis spectra of $I_3^-$ in seawater.showing rapid dismissing by the treatment of IPM-201

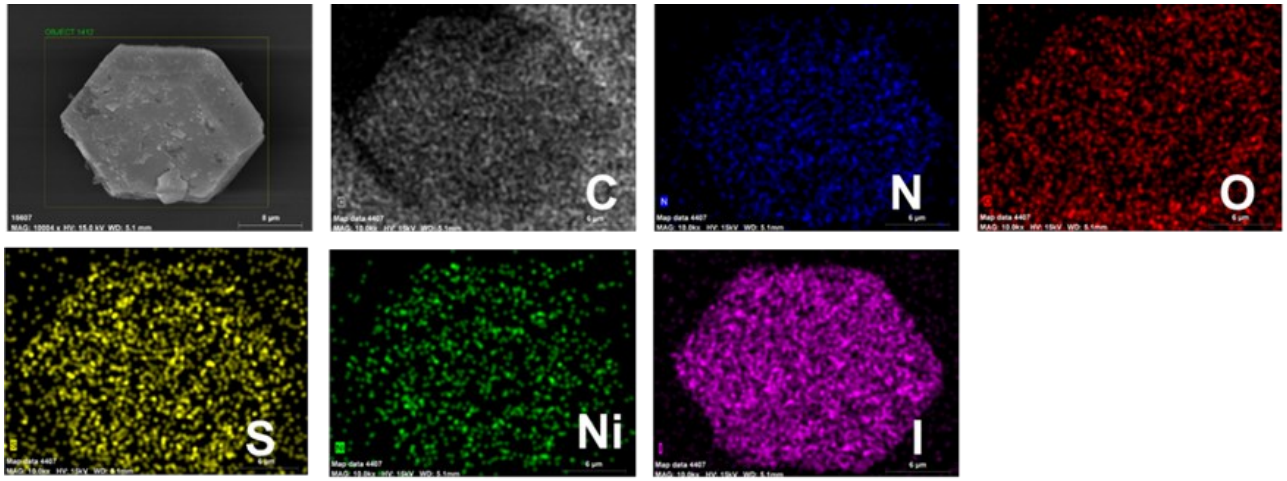


Appendix A15: FESEM elemental mapping image of IPM-201

| El | AN | Series | unn. C [wt.%] | norm. C [wt.%] | Atom. C [at.%] | Error (1 Sigma) [wt.%] |
|---|---|---|---|---|---|---|
| C | 6 | K-series | 31.80 | 67.97 | 82.14 | 3.95 |
| I | 53 | L-series | 6.37 | 13.61 | 1.56 | 0.25 |
| O | 8 | K-series | 4.89 | 10.46 | 9.49 | 0.98 |
| N | 7 | K-series | 2.84 | 6.06 | 6.28 | 0.88 |
| Ni | 28 | K-series | 0.74 | 1.57 | 0.39 | 0.09 |
| S | 16 | K-series | 0.15 | 0.32 | 0.14 | 0.04 |
| | | Total: | 46.79 | 100.00 | 100.00 | |

Table T1: EDX elemental analyses from the FESEM experiment of the IPM-201 show the presence of C, N, O, I, S, and Ni elements.

| El | AN | Series | unn. C [wt.%] | norm. C [wt.%] | Atom. C [at.%] | Error (1 Sigma) [wt.%] |
|---|---|---|---|---|---|---|
| C | 6 | K-series | 35.25 | 69.32 | 83.12 | 4.35 |
| I | 53 | L-series | 6.87 | 13.51 | 1.53 | 0.26 |
| O | 8 | K-series | 5.88 | 11.56 | 10.41 | 1.12 |
| N | 7 | K-series | 2.23 | 4.38 | 4.51 | 0.77 |
| S | 16 | K-series | 0.32 | 0.63 | 0.28 | 0.05 |
| Ni | 28 | K-series | 0.30 | 0.59 | 0.14 | 0.06 |
| | | Total: | 50.85 | 100.00 | 100.00 | |

Table T2: EDX elemental analyses from the FESEM experiment of the iMOF-3C show the presence of C, N, O, I, S, and Ni elements

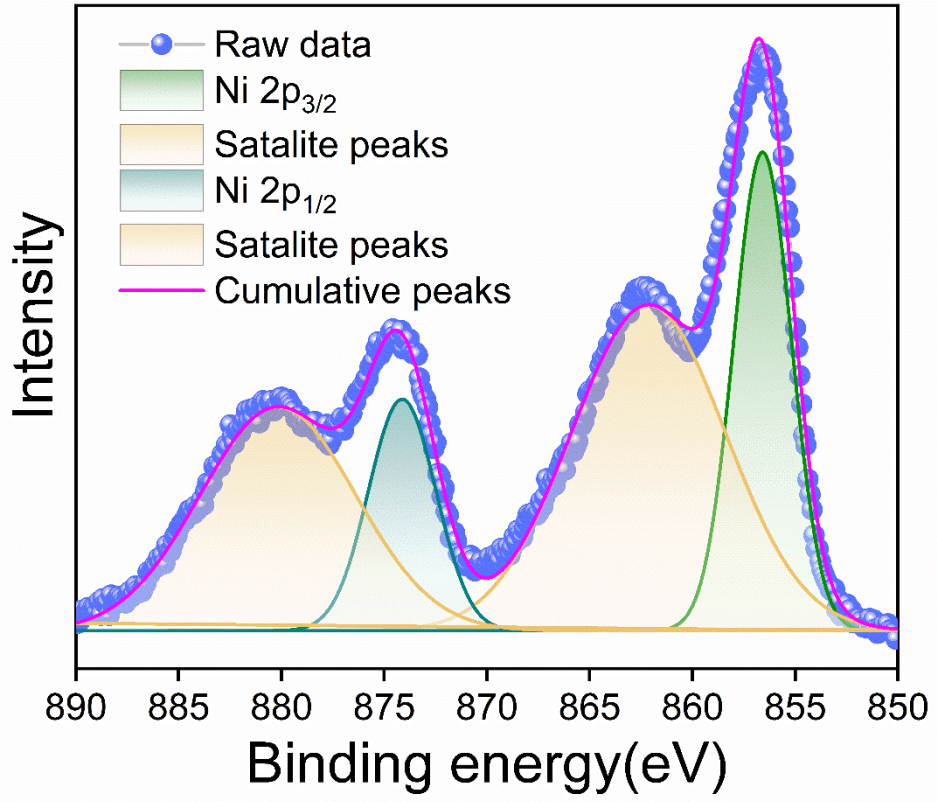


Appendix A16: Deconvoluted Ni 2p XPS of iMOF-3C

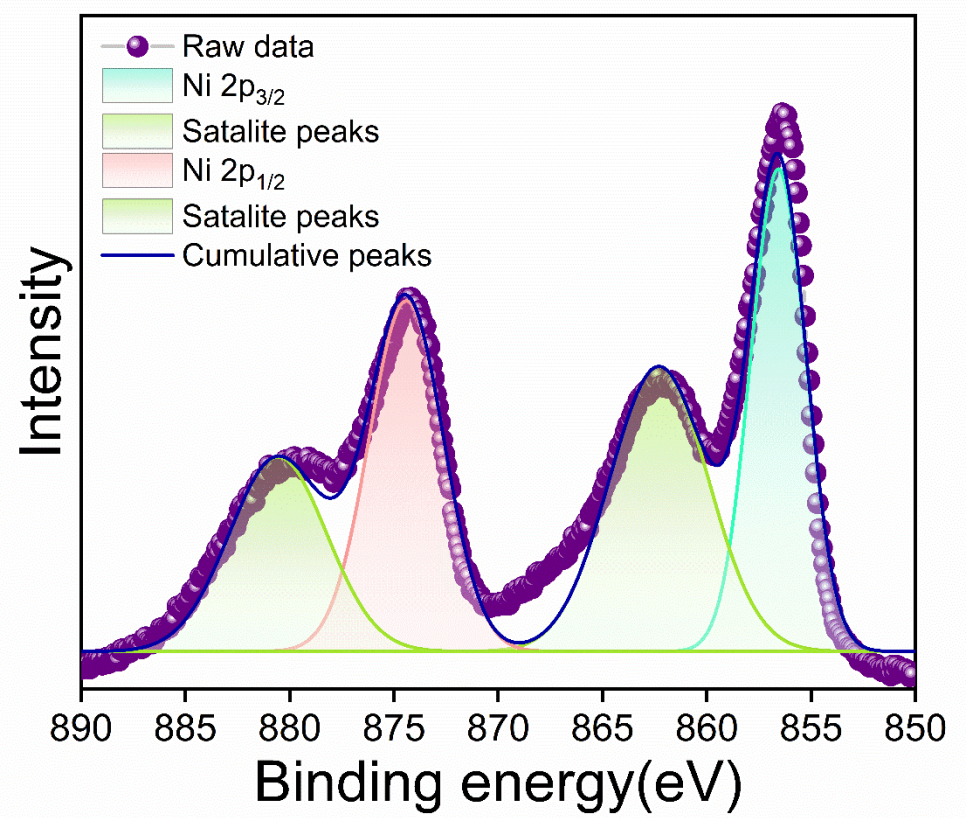


Appendix A17: Deconvoluted Ni 2p XPS of $I_2$@iMOF-3C

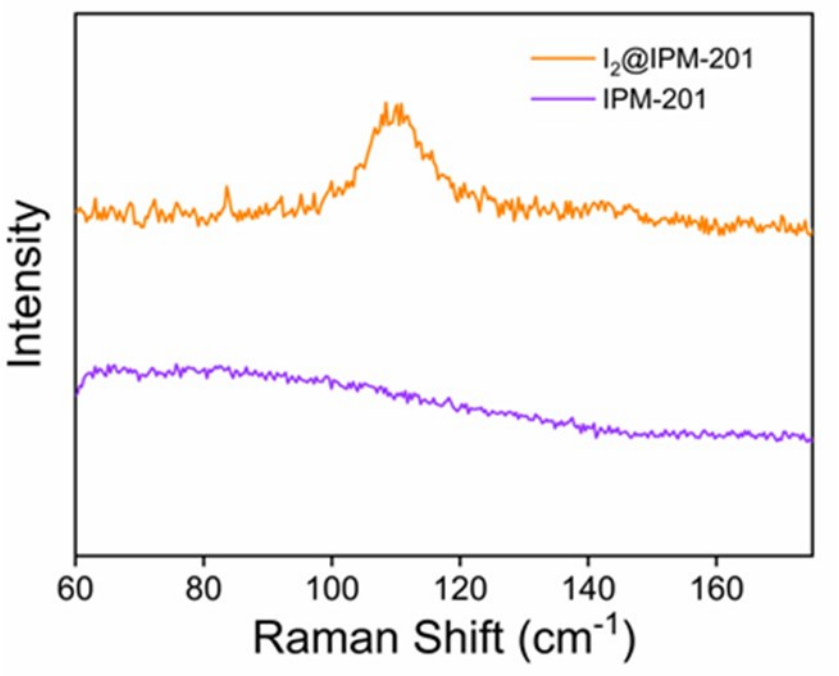


Appendix A18: Raman spectroscopy of pristine IPM-201 and loaded iodine IPM-201

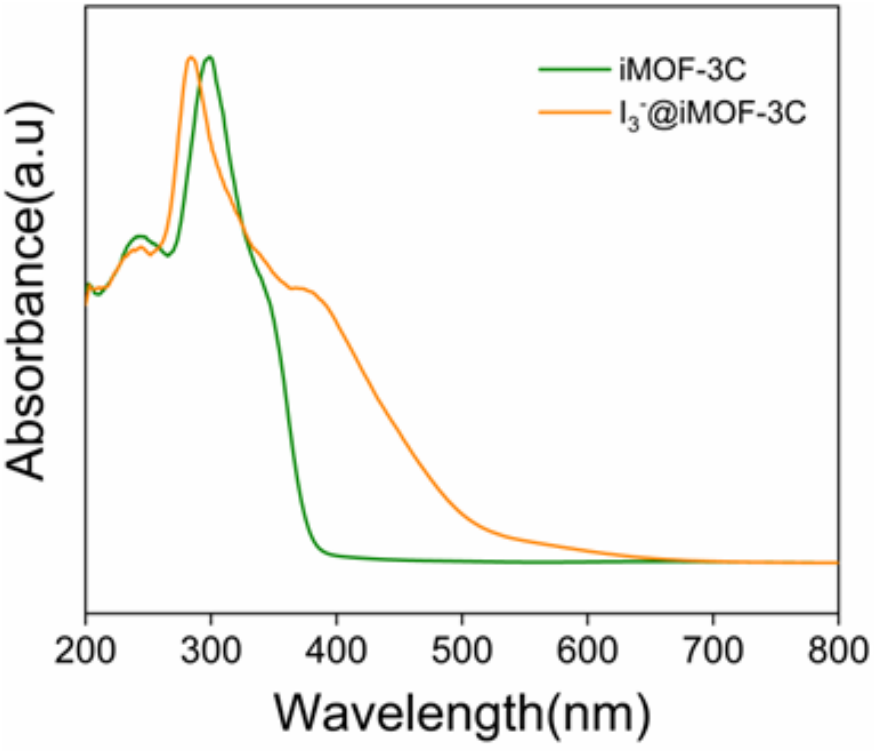


Appendix A19: Solid state UV-vis spectra of iMOF-3C and loaded $I_3^-$ iMOF-3C

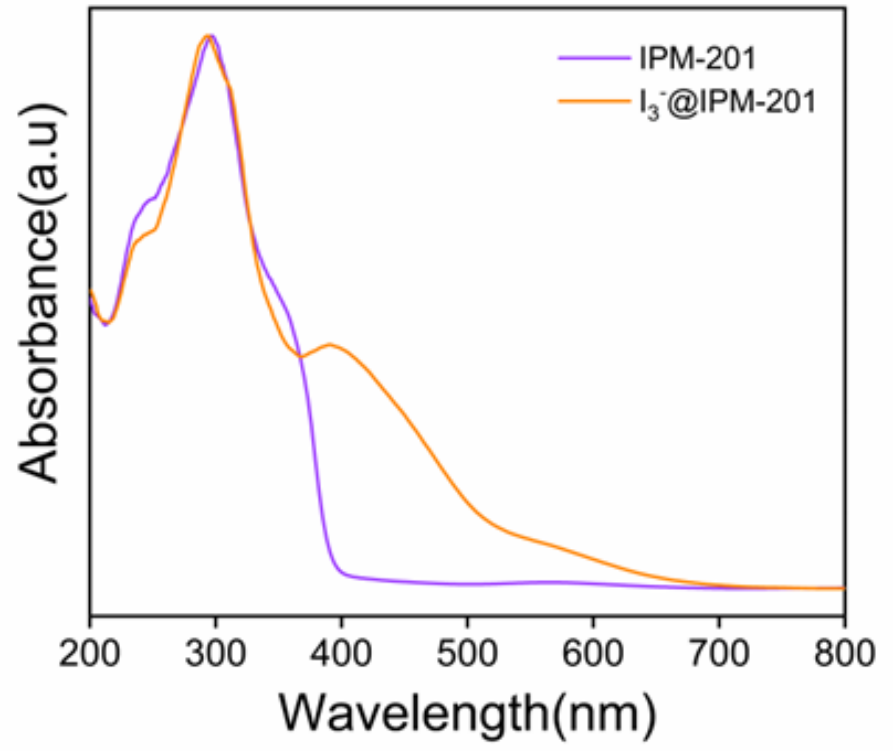


Appendix A20: Solid state UV-vis spectra of iMOF-3C and loaded $I_3^-$ iMOF-3C

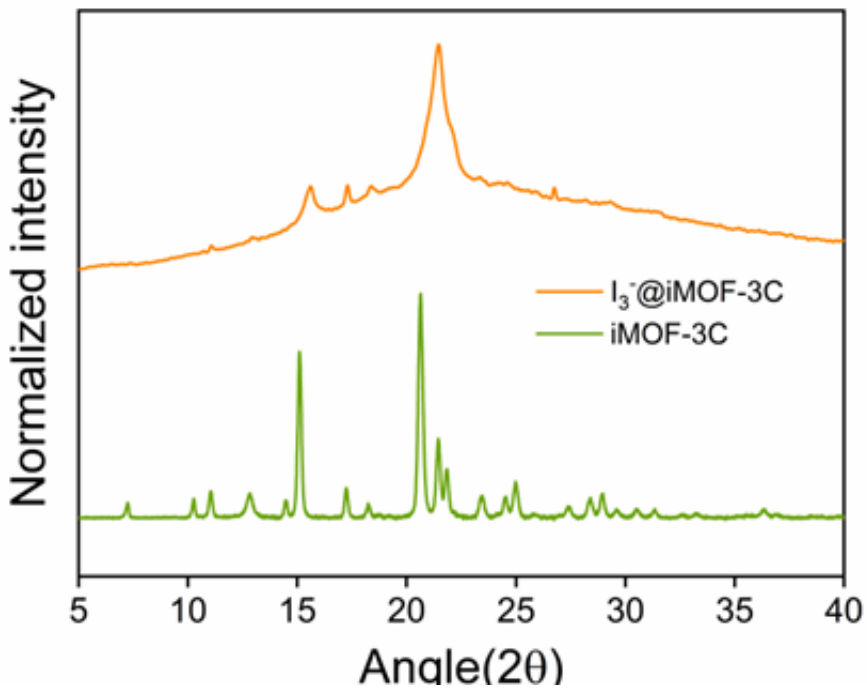


Appendix A21: PXRD of iMOF-3C before $I_3^-$ capture and after capture

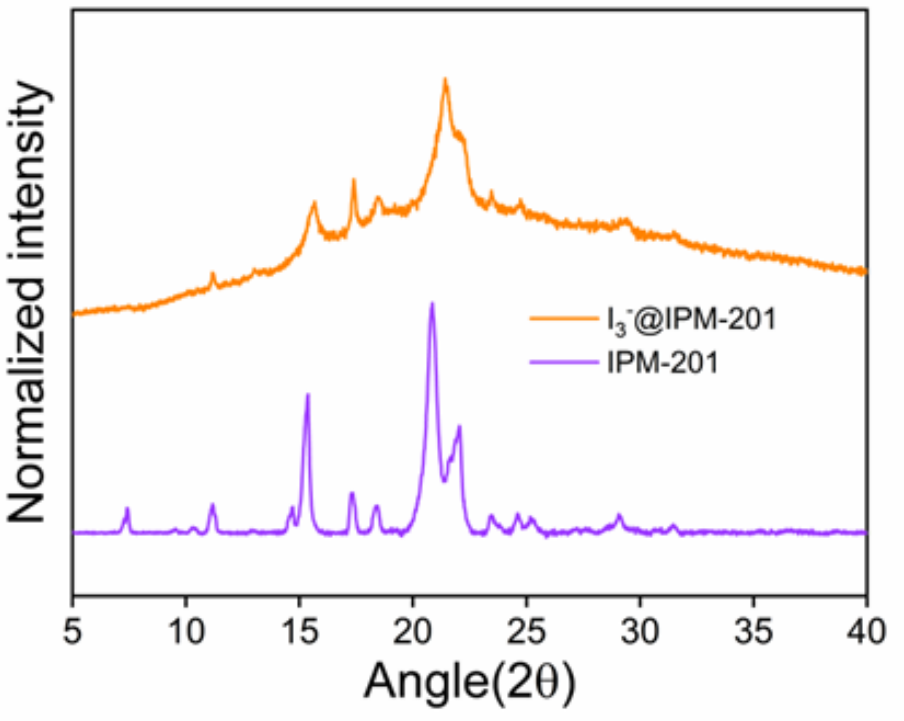


Appendix A22: PXRD of IPM-201 before $I_3^-$ capture and after capture

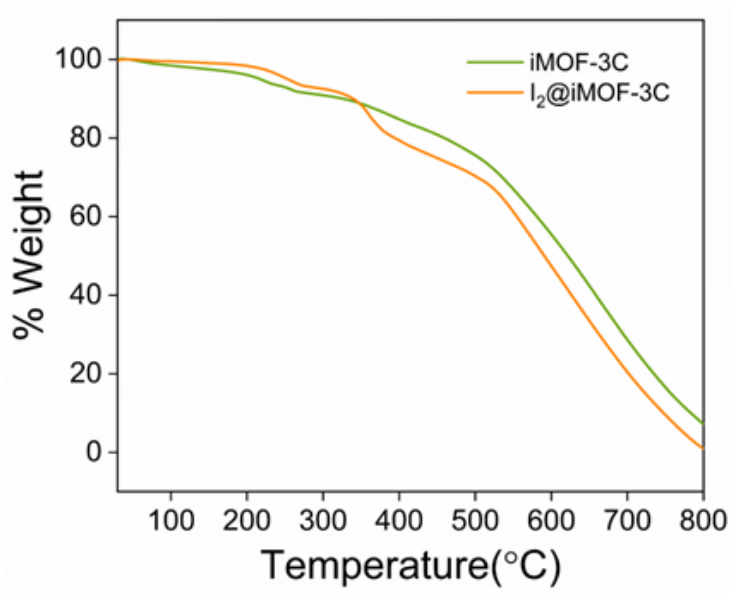


Appendix A23: TGA profile of iMOF-3C before and after iodine capture.

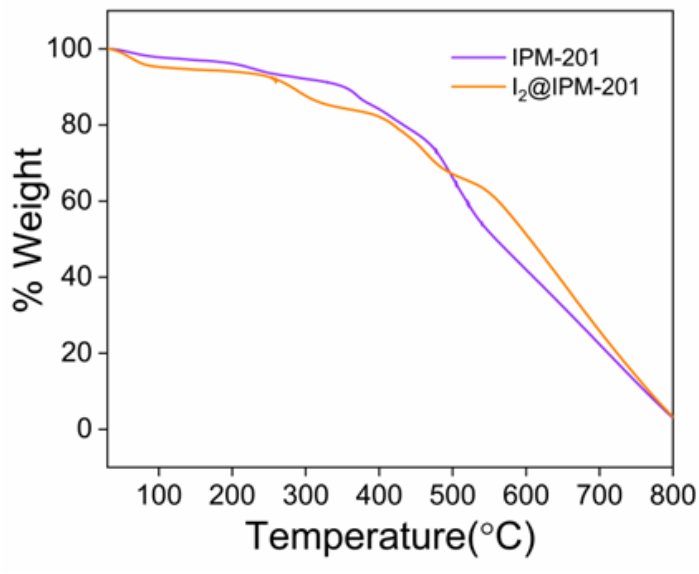


Appendix A24: TGA profile of iMOF-3C before and after iodine capture.

| MOFs | %C | %H | %N | %S |
|---|---|---|---|---|
| IPM-201 | 50.55 | 4.736 | 13.05 | 3.30 |
| $I_3^-$@IPM-201 | 34.69 | 2.66 | 9.03 | 2.31 |

Table T3: CHNS Elemental analysis of IPM-201 before and after $I_3^-$ capture.

| MOFs | %C | %H | %N | %S |
|---|---|---|---|---|
| iMOF-3C | 44.15 | 3.897 | 12.83 | 1.032 |
| $I_3^-$@iMOF-3C | 19.67 | 1.536 | 6.04 | 0.522 |

Table T4: CHNS Elemental analysis of iMOF-3C before and after I3- capture

# Reference


1. Day, G. S.; Drake, H. F.; Zhou, H.-C.; Ryder, M. R. Evolution of Porous Materials from Ancient Remedies to Modern Frameworks. *Commun. Chem*. **2021**, *4* (1), 114.
2. Valizadeh, B.; Nguyen, T. N.; Smit, B.; Stylianou, K. C. Porous Metal-Organic Framework@polymer Beads for Iodine Capture and Recovery Using a Gas-Sparged Column. *Adv. Funct. Mater*. **2018**, *28* (30), 1801596.
3. Saiz-Lopez, A.; Plane, J. M. C.; Baker, A. R.; Carpenter, L. J.; von Glasow, R.; Martín, J. C. G.; McFiggans, G.; Saunders, R. W. Atmospheric Chemistry of Iodine. *Chem. Rev*. **2012**, *112* (3), 1773–1804.
4. Riley, B. J.; Vienna, J. D.; Strachan, D. M.; McCloy, J. S.; Jerden, J. L., Jr. Materials and Processes for the Effective Capture and Immobilization of Radioiodine: *A Review. J. Nucl. Mater*. **2016**, *470*, 307–326.
5. Küpper, F. C.; Feiters, M. C.; Olofsson, B.; Kaiho, T.; Yanagida, S.; Zimmermann, M. B.; Carpenter, L. J.; Luther, G. W., 3rd; Lu, Z.; Jonsson, M.; Kloo, L. Commemorating Two Centuries of Iodine Research: An Interdisciplinary Overview of Current Research. *Angew. Chem. Int. Ed Engl*.
6. Zhou, W., Li, A., Zhou, M. *et al.* Nonporous amorphous superabsorbents for highly effective and selective adsorption of iodine in water. *Nat Commun* , **2023,***14* 5388 .
7. Ten Hoeve, J. E.; Jacobson, M. Z. Worldwide Health Effects of the Fukushima Daiichi Nuclear Accident. *Energy Environ. Sci*. **2012**, *5* (9), 8743.
8. Li, B.; Dong, X.; Wang, H.; Ma, D.; Tan, K.; Jensen, S.; Deibert, B. J.; Butler, J.; Cure, J.; Shi, Z.; Thonhauser, T.; Chabal, Y. J.; Han, Y.; Li, J. Capture of Organic Iodides from Nuclear Waste by Metal-Organic Framework-Based Molecular Traps. *Nat. Commun*. **2017**, *8* (1), 485.
9. Wang, J.; Li, Z.; Wang, Y.; Wei, C.; Ai, K.; Lu, L. Hydrogen Bond-Mediated Strong Adsorbent–I3− Interactions Enable High-Efficiency Radioiodine Capture. *Mater. Horiz*. **2019**, *6* (7), 1517–1525.
10. Xie, W.; Cui, D.; Zhang, S.-R.; Xu, Y.-H.; Jiang, D.-L. Iodine Capture in Porous Organic Polymers and Metal–Organic Frameworks Materials. *Mater. Horiz*. **2019**, *6* (8), 1571–1595.

11. Little, M. P.; Wakeford, R.; Bouville, A.; Simon, S. L. Measurement of Fukushima-Related Radioactive Contamination in Aquatic Species. Proc. Natl. *Acad. Sci. U. S. A*. **2016**, *113* (14), 3720–3721.
12. Sen, A.; Sharma, S.; Dutta, S.; Shirolkar, M. M.; Dam, G. K.; Let, S.; Ghosh, S. K. Functionalized Ionic Porous Organic Polymers Exhibiting High Iodine Uptake from Both the Vapor and Aqueous Medium. *ACS Appl. Mater. Interfaces* **2021**, *13* (29), 34188–34196.
13. Küpper, F. C.; Feiters, M. C.; Olofsson, B.; Kaiho, T.; Yanagida, S.; Zimmermann, M. B.; Carpenter, L. J.; Luther, G. W., 3rd; Lu, Z.; Jonsson, M.; Kloo, L. Commemorating Two Centuries of Iodine Research: An Interdisciplinary Overview of Current Research. *Angew. Chem. Int. Ed Engl*. **2011**, *50* (49), 11598–11620.
14. Svensson, P. H.; Kloo, L. Synthesis, Structure, and Bonding in Polyiodide and Metal Iodide-Iodine Systems. *Chem. Rev.* **2003**, *103* (5), 1649–1684.
15. Saiz-Lopez, A.; Plane, J. M. C.; Baker, A. R.; Carpenter, L. J.; von Glasow, R.; Martín, J. C. G.; McFiggans, G.; Saunders, R. W. Atmospheric Chemistry of Iodine. *Chem. Rev*. **2012**, *112* (3), 1773–1804.
16. Mushkacheva, G.; Rabinovich, E.; Privalov, V.; Povolotskaya, S.; Shorokhova, V.; Sokolova, S.; Turdakova, V.; Ryzhova, E.; Hall, P.; Schneider, A. B.; Preston, D. L.; Ron, E. Thyroid Abnormalities Associated with Protracted Childhood Exposure to 131I from Atmospheric Emissions from the Mayak Weapons Facility in Russia. *Radiat. Res*. **2006**, *166* (5), 715–722.
17. Guo, X.; Li, Y.; Zhang, M.; Cao, K.; Tian, Y.; Qi, Y.; Li, S.; Li, K.; Yu, X.; Ma, L. Colyliform Crystalline 2D Covalent Organic Frameworks (COFs) with Quasi-3D Topologies for Rapid I2 Adsorption. *Angew. Chem. Int. Ed Engl*. **2020**, *59* (50), 22697–22705
18. Huve, J.; Ryzhikov, A.; Nouali, H.; Lalia, V.; Augé, G.; Daou, T. J. Porous Sorbents for the Capture of Radioactive Iodine Compounds: *A Review. RSC Adv*. **2018**, *8* (51), 29248–29273
19. Jin, K.; Lee, B.; Park, J. Metal-Organic Frameworks as a Versatile Platform for Radionuclide Management. Coord. *Chem. Rev*. **2021**, *427* (213473), 213473.
20. Yang, Y.; Tu, C.; Yin, H.; Liu, J.; Cheng, F.; Luo, F. Molecular Iodine Capture by Covalent Organic Frameworks. *Molecules* **2022**, 27 (24), 9045.

21. Robshaw, T. J.; Turner, J.; Kearney, S.; Walkley, B.; Sharrad, C. A.; Ogden, M. D. Capture of Aqueous Radioiodine Species by Metallated Adsorbents from Wastestreams of the Nuclear Power Industry: *A Review. SN Appl. Sci*. **2021**, *3* (11)
22. Yu, Y.-N.; Yin, Z.; Cao, L.-H.; Ma, Y.-M. Organic Porous Solid as Promising Iodine Capture Materials. J. Incl. Phenom. Macrocycl*. Chem*. **2022**, *102* (5–6), 395–427.
23. Zhang, X.; Maddock, J.; Nenoff, T. M.; Denecke, M. A.; Yang, S.; Schröder, M. Adsorption of Iodine in Metal-Organic Framework Materials*. Chem. Soc. Rev*. **2022**, *51* (8), 3243–3262.
24. Zhang, X.; da Silva, I.; Godfrey, H. G. W.; Callear, S. K.; Sapchenko, S. A.; Cheng, Y.; Vitórica-Yrezábal, I.; Frogley, M. D.; Cinque, G.; Tang, C. C.; Giacobbe, C.; Dejoie, C.; Rudić, S.; Ramirez-Cuesta, A. J.; Denecke, M. A.; Yang, S.; Schröder, M. Confinement of Iodine Molecules into Triple-Helical Chains within Robust Metal-Organic Frameworks. *J. Am. Chem*. *Soc.* **2017**, *139* (45), 16289–16296.
25. Gogia, A.; Das, P.; Mandal, S. K. Tunable Strategies Involving Flexibility and Angularity of Dual Linkers for a 3D Metal-Organic Framework Capable of Multimedia Iodine Capture. *ACS Appl. Mater. Interfaces* **2020**, *12* (41), 46107–46118.
26. Wang, G.-Q.; Huang, J.-F.; Huang, X.-F.; Deng, S.-Q.; Zheng, S.-R.; Cai, S.-L.; Fan, J.; Zhang, W.-G. A Hydrolytically Stable Cage-Based Metal–Organic Framework Containing Two Types of Building Blocks for the Adsorption of Iodine and Dyes. *Inorg. Chem. Front*. **2021**, *8* (4), 1083–1092.
27. Guo, X.; Li, Y.; Zhang, M.; Cao, K.; Tian, Y.; Qi, Y.; Li, S.; Li, K.; Yu, X.; Ma, L. Colyliform Crystalline 2D Covalent Organic Frameworks (COFs) with Quasi-3D Topologies for Rapid I2 Adsorption. *Angew. Chem*. *Int. Ed Engl.* **2020,** *59* (50), 22697–22705.
28. Li, J.; Zhang, H.; Zhang, L.; Wang, K.; Wang, Z.; Liu, G.; Zhao, Y.; Zeng, Y. Two-Dimensional Covalent–Organic Frameworks for Ultrahigh Iodine Capture. *J. Mater. Chem. A Mater. Energy Sustain.* **2020**, *8* (19), 9523–9527.
29. Xie, Y.; Pan, T.; Lei, Q.; Chen, C.; Dong, X.; Yuan, Y.; Shen, J.; Cai, Y.; Zhou, C.; Pinnau, I.; Han, Y. Ionic Functionalization of Multivariate Covalent Organic

Frameworks to Achieve an Exceptionally High Iodine-capture Capacity. *Angew. Chem. Weinheim Bergstr. Ger.* **2021**, *133* (41), 22606–22614

30. Tian, X.; Zhou, G.; Xi, J.; Sun, R.; Zhang, X.; Wang, G.; Mei, L.; Hou, C.; Jiang, L.; Qiu, J. Vinyl-Functionalized Covalent Organic Frameworks for Effective Radioactive Iodine Capture in Aqueous Solution. *Sep. Purif. Technol*. **2023**, *310* (123160), 123160.
31. Yan, Z.; Yuan, Y.; Tian, Y.; Zhang, D.; Zhu, G. Addendum: Highly Efficient Enrichment of Volatile Iodine by Charged Porous Aromatic Frameworks with Three Sorption Sites. *Angew. Chem. Weinheim Bergstr. Ger*. **2015**, *127* (48), 14422–14422.
32. Xie, L.; Zheng, Z.; Lin, Q.; Zhou, H.; Ji, X.; Sessler, J. L.; Wang, H. Calix[4]Pyrrole-Based Crosslinked Polymer Networks for Highly Effective Iodine Adsorption from Water. *Angew. Chem. Int. Ed Engl*. **2022**, *61* (1), e202113724.
33. Dai, D.; Yang, J.; Zou, Y.-C.; Wu, J.-R.; Tan, L.-L.; Wang, Y.; Li, B.; Lu, T.; Wang, B.; Yang, Y.-W. Macrocyclic Arenes-Based Conjugated Macrocycle Polymers for Highly Selective CO2 Capture and Iodine Adsorption. *Angew. Chem. Int. Ed Engl*. **2021**, *60* (16), 8967–8975.
34. Zhang, M.; Samanta, J.; Atterberry, B. A.; Staples, R.; Rossini, A. J.; Ke, C. A Crosslinked Ionic Organic Framework for Efficient Iodine and Iodide Remediation in Water. *Angew. Chem. Int. Ed Engl*. **2022**, *61* (52), e202214189.
35. Dam, G. K.; Fajal, S.; Dutta, S.; Let, S.; Desai, A. V.; Ghosh, S. K. Hydrolytically Stable Luminescent Cationic MOF for Selective Detection of Toxic Organic Arsenic in Water. *ACS Appl. Opt. Mater*. **2023**, *1* (7), 1217–1226.
36. Sharma, S.; Let, S.; Desai, A. V.; Dutta, S.; Karuppasamy, G.; Shirolkar, M. M.; Babarao, R.; Ghosh, S. K. Rapid, Selective Capture of Toxic Oxo-Anions of Se(Iv), Se(vi) and As(v) from Water by an Ionic Metal–Organic Framework (iMOF). *J. Mater. Chem. A Mater. Energy Sustain*. **2021**, *9* (10), 6499–6507.
37. Desai, A. V.; Roy, A.; Samanta, P.; Manna, B.; Ghosh, S. K. Base-Resistant Ionic Metal-Organic Framework as a Porous Ion-Exchange Sorbent. *iScience* **2018**, *3*, 21–30.
38. Sharma, S.; Let, S.; Desai, A. V.; Dutta, S.; Karuppasamy, G.; Shirolkar, M. M.; Babarao, R.; Ghosh, S. K. Rapid, Selective Capture of Toxic Oxo-Anions of

Se(Iv), Se(vi) and As(v) from Water by an Ionic Metal–Organic Framework (iMOF). *J. Mater. Chem. A Mater. Energy Sustain*. **2021**, *9* (10), 6499–6507.